

On the statistical assumption on the distance moduli of Supernovae Ia and its impact on the determination of cosmological parameters

M.G. Dainotti^{a,b,c,d,*}, G. Bargiacchi^{e,f}, M. Bogdan^{g,h}, S. Capozziello^{e,f,i}, S. Nagataki^{j,k,l}

^aNational Astronomical Observatory of Japan, 2 Chome-21-1 Osawa, Mitaka, Tokyo, 181-8588, Japan

^bThe Graduate University for Advanced Studies, SOKENDAI, Shonankokusaimura, Hayama, Miura District, Kanagawa, 240-0193, Japan

^cSpace Science Institute, 4765 Walnut St, Suite B, Boulder, 80301, Colorado, USA

^dDepartment of Physics and Astrophysics, University of Las Vegas, 89154, USA

^eScuola Superiore Meridionale, Largo S. Marcellino 10, Naples, 80138, Italy

^fIstituto Nazionale di Fisica Nucleare (INFN), Sez. di Napoli, Complesso Univ. Monte S. Angelo, Via Cinthia 9, Naples, 80126, Italy

^gUniversity of Wrocław, plac Grunwaldzki 2/4, Wrocław, 50-384, Poland

^hDepartment of Statistics, Lund University, Box 117, SE-221 00, Lund, Sweden

ⁱDipartimento di Fisica "E. Pancini", Università degli Studi di Napoli Federico II, Complesso Univ. Monte S. Angelo, Via Cinthia 9, Naples, 80126, Italy

^jInterdisciplinary Theoretical & Mathematical Science Program, RIKEN (iTHEMS), 2-1 Hirosawa, Wako, Saitama, 351-0198, Japan

^kRIKEN Cluster for Pioneering Research, Astrophysical Big Bang Laboratory (ABBL), 2-1 Hirosawa, Wako, Saitama, 351-0198, Japan

^lAstrophysical Big Bang Group (ABBG), Okinawa Institute of Science and Technology Graduate University (OIST), 1919-1 Tancha, Okinawa, 904-0495, Japan

Abstract

Type Ia Supernovae (SNe Ia) are considered the most reliable *standard candles* and they have played an invaluable role in cosmology since the discovery of the Universe's accelerated expansion. During the last decades, the SNe Ia samples have been improved in number, redshift coverage, calibration methodology, and systematics treatment. These efforts led to the most recent "Pantheon" (2018) and "Pantheon+" (2022) releases, which enable to constrain cosmological parameters more precisely than previous samples. In this era of precision cosmology, the community strives to find new ways to reduce uncertainties on cosmological parameters. To this end, we start our investigation even from the likelihood assumption of Gaussianity, implicitly used in this domain. Indeed, the usual practise involves constraining parameters through a Gaussian distance moduli likelihood. This method relies on the implicit assumption that the difference between the distance moduli measured and the ones expected from the cosmological model is Gaussianly distributed. In this work, we test this hypothesis for both the *Pantheon* and *Pantheon+* releases. We find that in both cases this requirement is not fulfilled and the actual underlying distributions are a logistic and a Student's t distribution for the *Pantheon* and *Pantheon+* data, respectively. When we apply these new likelihoods fitting a flat Λ CDM model, we significantly reduce the uncertainties on the matter density Ω_M and the Hubble constant H_0 of $\sim 40\%$. As a result, the Hubble tension is increased at $> 5\sigma$ level. This boosts the SNe Ia power in constraining cosmological parameters, thus representing a huge step forward to shed light on the current debated tensions in cosmology.

Keywords: Type Ia supernovae, Statistics, Cosmological parameters, Cosmology

1. Introduction

The most accredited Universe parametrization is the Λ CDM model (Peebles, 1984), which includes a cold dark matter (CDM) component and a cosmological constant Λ (Carroll, 2001), as suggested by the Universe accelerated expansion (Riess et al., 1998; Perlmutter et al., 1999). Predictions from this scenario are compatible with the cosmic microwave background (CMB; Planck Collaboration et al., 2020), the baryon acoustic oscillations (Alam et al., 2021), and type Ia Supernovae (SNe Ia). Nevertheless, the Λ CDM model suffers from theoretical and observational shortcomings: the cosmological constant problem (Weinberg, 1989), the fine-tuning, the origin and properties of dark energy, and the Hubble constant (H_0) tension, which is the discrepancy between the H_0 value obtained from the Planck data of the CMB within a flat Λ CDM

model ($H_0 = 67.4 \pm 0.5 \text{ km s}^{-1} \text{ Mpc}^{-1}$, Planck Collaboration et al. 2020), and the local H_0 from SNe Ia and Cepheids ($H_0 = 73.04 \pm 1.04 \text{ km s}^{-1} \text{ Mpc}^{-1}$, Riess et al. 2022). This discrepancy varies from 4.4 to 6 σ when different samples are considered (Riess et al., 2019; Camarena and Marra, 2020; Wong et al., 2020). Time-delay and strong lensing from quasars (Liao et al., 2019) provide a value close to SNe Ia, while cosmic chronometers favour the H_0 of the CMB (Gómez-Valent and Amendola, 2018). Instead, quasars (Risaliti and Lusso, 2019; Lusso et al., 2020; Lenart et al., 2023), the Tip of the Red-Giant Branch (Freedman, 2021), and Gamma-ray bursts (Cardone et al., 2009, 2010; Dainotti et al., 2013; Postnikov et al., 2014; Dainotti et al., 2021, 2022a,b,c), hint at a H_0 value halfway between these two. So, the H_0 tension remains an open question. One way to better highlight the tension is to reduce H_0 uncertainty. As a first step towards this goal, we have questioned the Gaussianity assumption on the likelihood traditionally used for SNe Ia. Indeed, the common practise of constraining cosmo-

*The first and second author have contributed equally to the paper. Corresponding author, maria.dainotti@nao.ac.jp.

logical parameters with a Gaussian distance moduli likelihood, \mathcal{L}_{Gauss} , relies on the implicit assumption that the difference between the distance moduli, μ , measured and expected from a cosmological model, normalized to the uncertainty, is normally distributed. Nonetheless, the weak lensing effect should cause a skew in the supernova magnitude distribution, which increases with redshift, thus leading to a non-Gaussianity of the supernova distribution (Holz and Linder, 2005). As a consequence, the amount of skewness can be also used to measure the amount of lensing, and test whether it is consistent with the measured clustering, as shown in Amendola et al. (2010); Jönsson et al. (2010); Smith et al. (2014); Macaulay et al. (2020). In this scenario of non-Gaussianity, the appropriate choice for the cosmological likelihood is crucial to obtain statistically reliable results and better constrain cosmological parameters, reducing their uncertainties. Hence, we here investigate this assumption, for the *Pantheon* (Scolnic et al., 2018) and *Pantheon +* (Scolnic et al., 2022) samples, determining the best-fit likelihoods which we then employ to properly perform a cosmological study and constrain cosmological parameters with each of the SNe Ia data.

The manuscript is composed as follows. Section 2.1 introduces the SNe Ia samples and the use of distance moduli in SNe Ia cosmology. Then, Section 2.2 details the Gaussianity assumption along with the Gaussianity tests performed. Section 2.3 describes the fitting procedure. In Section 3, we describe the results both for the best-fit likelihoods and their cosmological application. In Section 4 we draw our conclusions. In Appendix A we test the reliability of our results through mock samples.

2. Methodology

2.1. Data and the distance moduli

We use the “*Pantheon*” (Scolnic et al., 2018) and the “*Pantheon +*” (Scolnic et al., 2022) samples considering the covariance matrix with statistical and systematic uncertainties. The first includes 1048 sources in the redshift range $z = 0.01 - 2.26$, from CfA1-4, *Carnegie Supernova Project*, *Pan-STARRS1*, *Sloan Digital Sky Survey*, *Supernova Legacy Survey*, and *Hubble Space Telescope*, the latter counts 1701 SNe Ia from 18 different surveys in the range $z = 0.001 - 2.26$. The *Pantheon +* sample has an increased redshift span, and number of sources at low redshift, and an enriched treatment of systematic uncertainties. The “*Pantheon+*” contains 753 more SNe Ia compared to the *Pantheon* which are not present in the *Pantheon*, while the *Pantheon* sample has 182 SNe Ia which are not included in the “*Pantheon+*”. These improvements enable better constraints on cosmological parameters (Brout et al., 2022). We use both samples to investigate how and to what extent our analysis is impacted by the above-mentioned changes in the SNe Ia sample.

To apply SNe Ia as cosmological tools, we compute the difference between the observed and the theoretical distance moduli, μ . The observed μ is

$$\mu_{obs} = m_B - M + \alpha x_1 - \beta c + \Delta_M + \Delta_B \quad (1)$$

where m_B is the B-band overall amplitude, x_1 the stretch parameter, c the color, α and β the coefficients of the relation of luminosity with x_1 and c , respectively, M the fiducial B-band absolute magnitude of a SN with $x_1 = 0$ and $c = 0$, Δ_M and Δ_B the corrections on the distance accounting for host-galaxy mass and biases, predicted through simulations, respectively (Scolnic et al., 2018, 2022). SNe Ia alone cannot determine H_0 , as it is degenerate with M , whereas M depends on biases, contributions to statistical and systematic errors, etc. (Scolnic et al., 2018). Nevertheless, H_0 can be derived by fixing M . Usually, Cepheids are used to determine M (Brout et al., 2022; Riess et al., 2022). Scolnic et al. (2018) fix $M = -19.35$, as can be derived by the inversion of Eq. (1), implying $H_0 = 70 \text{ km s}^{-1} \text{ Mpc}^{-1}$ (Dainotti et al., 2021, 2022a). Riess et al. (2022) obtain $M = -19.253 \pm 0.027$ and $H_0 = 73.04 \pm 1.04 \text{ km s}^{-1} \text{ Mpc}^{-1}$ combining 42 SNe Ia with a sample of Cepheids hosted by the same galaxies. This value of M is assumed to compute μ for the *Pantheon +*. The theoretical μ , assuming a flat Λ CDM model and omitting the current relativistic density parameter, negligible in the late Universe, is (Kenworthy et al., 2019):

$$\begin{aligned} \mu_{th} &= 5 \log_{10} d_l(\text{Mpc}) + 25 \\ &= 5 (1 + z_{hel}) \frac{c}{H_0} \int_0^{z_{HD}} \frac{dz'}{\sqrt{\Omega_M (1+z)^3 + (1 - \Omega_M)}} + 25 \end{aligned} \quad (2)$$

where d_l is the luminosity distance, c the light speed, Ω_M the current matter density, z_{hel} the redshift in the heliocentric frame, and z_{HD} the redshift corrected for CMB dipole motion and peculiar velocity. We are aware that the formula in Equation 2 properly works at low redshifts, as in Kenworthy et al. (2019), where the SNe Ia sample investigated covers only $z < 0.08$, but could not be suitable for *Pantheon* and *Pantheon +* samples, which reach $z = 2.26$. Hence, we perform all our analysis by applying both Equation 2 and the same equation in which z_{hel} is replaced by z_{HD} . The latter reads as:

$$\mu_{th} = 5 (1 + z_{HD}) \frac{c}{H_0} \int_0^{z_{HD}} \frac{dz'}{\sqrt{\Omega_M (1+z)^3 + (1 - \Omega_M)}} + 25. \quad (3)$$

This allows us to compare the results obtained with the two different formula to compute μ_{th} . In Scolnic et al. (2018) for the evaluation of cosmological parameters the χ^2 is defined as

$$\chi^2 = \Delta\mu^T C^{-1} \Delta\mu \quad (4)$$

where $\Delta\mu = \mu_{th} - \mu_{obs}$ and C is the uncertainty matrix built as $C = D_{stat} + C_{sys}$, with D_{stat} the diagonal matrix with statistical errors and C_{sys} the systematic covariance matrix, both provided by SNe Ia releases (Scolnic et al., 2018; Brout et al., 2022; Scolnic et al., 2022). As a consequence, we are considering for each measurement its individual distance uncertainties, since different SNe Ia light-curves present different quality, signal-to-noise ratio, and contributions to the overall uncertainty, as detailed in Scolnic et al. (2022). We here stress that we have considered both the systematic and statistical uncertainty to guarantee more

reliable confidence levels of the cosmological parameters. Indeed, the C_{sys} matrix is defined through a sum over the sources as follows

$$C_{ij,\text{sys}} = \sum_{k=1}^K \left(\frac{\delta\mu_i}{\delta S_k} \right) \left(\frac{\delta\mu_j}{\delta S_k} \right) (\sigma_{S_k})^2 \quad (5)$$

where k runs over the systematic S_k , σ_{S_k} is the magnitude of each systematic error, and $\delta\mu$ is computed as the binned difference in distances when changing one of the systematic parameters.

2.2. The Gaussianity assumption in the likelihood

It is common practise to apply a Gaussian cosmological likelihood for SNe Ia. However, often the Gaussianity statement is not carefully checked each time or once the sample is enlarged. We investigate if the argument $\Delta\mu_{\text{norm}} = C^{-1/2} \Delta\mu$ (Lovick et al., 2023) of the likelihood of SNe Ia distance moduli (\mathcal{L}) in the *Pantheon* and *Pantheon+* fulfills the Gaussianity condition within a flat Λ CDM model with $\Omega_M = 0.3$ and $H_0 = 70 \text{ km s}^{-1} \text{ Mpc}^{-1}$. We define $\Delta\mu_{\text{norm}}$ this way to investigate the normalised residuals of the distance moduli while accounting for both the diagonal and the non-diagonal terms of the C matrix, which include both statistical and systematic uncertainties. Nevertheless, we have also tested that, if we do not consider the non-diagonal terms of the C matrix, thus considering only $\Delta\mu/\sigma_\mu$, where σ_μ is the diagonal part of C , our results on the Gaussianity assumption, and hence our cosmological results, do not change. Since the computation of $\Delta\mu_{\text{norm}}$ requires the assumption of a specific cosmological model, we have chosen to report here the results obtained assuming a flat Λ CDM model with $\Omega_M = 0.3$ and $H_0 = 70 \text{ km s}^{-1} \text{ Mpc}^{-1}$. Indeed, this value of Ω_M is the one reported in Scolnic et al. (2018) and the value of $H_0 = 70 \text{ km s}^{-1} \text{ Mpc}^{-1}$ is the one obtained in several works that combine SNe Ia with other probes (e.g. Di Valentino et al., 2020; Cao et al., 2021; Abdalla et al., 2022). We here notice that we have checked the impact of this cosmological assumption on our results by computing the distribution of $\Delta\mu_{\text{norm}}$ by imposing other values of Ω_M . More specifically, we have tested the two extreme cases of $\Omega_M = 0.1$ and $\Omega_M = 1$. Under these new assumptions, as expected, the values of skewness and kurtosis of the distribution of $\Delta\mu_{\text{norm}}$ change. Nevertheless, both *Pantheon* and *Pantheon+* data still fail all the Gaussianity tests employed in our analysis and remarkably the best-fit distributions are still a logistic and a Student's T, respectively. Hence, our results on the Gaussianity tests (Sect. 3.1) and new best-fit likelihoods (Sect. 3.2), as well as the cosmological results reported in Sect. 3.3, do not depend on the assumption of a flat Λ CDM model with $\Omega_M = 0.3$ and $H_0 = 70 \text{ km s}^{-1} \text{ Mpc}^{-1}$.

We apply several methods to test if $\Delta\mu_{\text{norm}}$ is normally distributed. We have applied all the tests to all individual data points of $\Delta\mu_{\text{norm}}$ and not in bins. μ_{obs} in Equation (1) is taken directly from Scolnic et al. (2018)¹ and Scolnic et al. (2022)², while μ_{th} is specified in Eq. (2). When the likelihood is

Gaussian there is the implicit assumption that the residual, the argument in the formula of the likelihood ($\Delta\mu_{\text{norm}}$ in Eq. (6)), must be Gaussian. As anticipated, due to the weak lensing effect the distribution is not expected to be Gaussian (Holz and Linder, 2005). Moreover, the discussion about Gaussianity in the large structure analysis has been already treated in Hahn et al. (2019) along with the impact of the Gaussian assumption on cosmological parameters. In this regard, some studies concerning to what extent the non-Gaussianity could affect the determination of the cosmological parameters have already been performed (Sarkar et al., 2008; Shah et al., 2023). Moreover, possibilities to use non-Gaussian approaches for SNe Ia and Cepheids gathered by Riess et al. (2016) and Pantheon+ have been also studied in Feeney et al. (2018) and Keeley et al. (2022), respectively, but we here for the first time perform a comparative analysis with the Pantheon and Pantheon+ sample.

We apply the Anderson-Darling (Stephens, 1976, 1979) and Shapiro-Wilk (Shapiro and Wilk, 1965) normality tests, and we compute skewness and kurtosis of the distributions, the skewness (D'agostino et al., 1990), the kurtosis (Anscombe and Glynn, 1983) and a test that combines both features (D'Agostino and Pearson, 1973)³. The Anderson-Darling and Shapiro-Wilk tests determine whether a data sample is drawn from the Gaussian distribution, and they are frequently applied in the literature (e.g. Dainotti et al. 2022d in astrophysics and Stephens 1974; Razali et al. 2011 in statistics). An important property of these tests is their consistency: they can identify any small deviation from normality, if the sample size is large enough (Stephens, 1976; Leslie et al., 1986). Therefore, the larger the sample size, the more these tests tend to reject the null hypothesis of normal distribution (Yazici and Yolacan, 2007), even in case of very small deviations from Gaussianity such as in presence of ties caused by limited measurement precision (i.e. the number of decimals). This weakness limits the applicability of the Anderson-Darling and Shapiro-Wilk tests on large samples and must be accounted for when considering SNe Ia samples that count more than 1000 sources. Thus, we include investigations on skewness and kurtosis. The skewness is the third standardized moment and measures the asymmetry of the distribution as it identifies extreme values in one tail versus the other. The kurtosis is the fourth standardized moment and measures extreme values in both tails: large kurtosis corresponds to more populated tails than the ones of a Gaussian distribution, small kurtosis to less populated tails than the ones of a Gaussian distribution. A normal distribution has skewness and kurtosis equal to zero⁴. So, the skewness and kurtosis of a distribution provide information on the deviation from normality. Based on this, we use the skewness and kurtosis tests, to determine if the values of skewness and kurtosis of the investigated distribution are so statistically close to zero, that it can be well approximated by a Gaussian distribution. Furthermore, we apply the ‘‘skewness+kurtosis’’ test, which contemporaneously checks departures of skewness and kurtosis from Gaussians. These

³These analyses are performed with the scipy Python package.

⁴We consider Fisher's definition of kurtosis, in which 3 is subtracted from the result to give 0 for a normal distribution.

¹<https://github.com/dscolnic/Pantheon>

²<https://github.com/PantheonPlusSH0ES>

complementary methods are crucial to obtain reliable results on the investigation of the Gaussianity assumption on the SNe Ia $\Delta\mu_{norm}$.

2.3. Fit with the new likelihoods

Since the tests described above fail (Sec. 3.1), we further extend our analysis. First, we fit the $\Delta\mu_{norm}$ values to find the best-fit distribution with the Mathematica tool FindDistribution which finds the best distributions among the first 20 best-fitting distributions. We have checked the reliability of these results with python as well. More specifically, we have employed the Mathematica tool by requiring that each distribution investigated is compared with the others through all possible properties evaluated by FindDistribution, among which there are (see also Section 3.2) the logarithm of the likelihood value, the Bayesian Information Criterion (BIC), the Akaike Information Criterion (AIC), and the p-values of the Pearson χ^2 and Cramer Von Mises tests. After this comparison, the fitting distributions are determined starting from the best-fit one to the ones that reproduce the data with highest accuracy. We report in Table 1, the first five fitting distributions for both *Pantheon* and *Pantheon +* samples along with the corresponding values of the above-mentioned statistical tests. Indeed, the value of the likelihood and the BIC, and AIC criteria provide an estimate of the quality of the statistical model investigated for a given set of data. More precisely, larger values of likelihood and lower values of BIC and AIC identify the favored model. We here notice that we show in Table 1 the values of BIC and AIC computed with python. Indeed, python follows the standard definition and notation for these two criteria. This allows a more immediate and easier interpretation of the table since the preferred models are the ones with lower BIC and AIC. Additionally, the Pearson χ^2 and the Cramer Von Mises tests include, respectively, the Pearson and Cramer Von Mises goodness-of-fit tests with null hypothesis that the data is drawn from a population with a specific distribution. For these tests, if the p-value is small enough (usually $p < 0.05$ by convention), then the null hypothesis is rejected, and we conclude that the observed data does not follow that distribution. Thus, in these tests, the distributions with larger p-values are the preferred ones. The distribution here used is the first best-fit distribution shown in Table 1.

The found distribution is used in \mathcal{L} (\mathcal{L}_{new}) instead of the Gaussian probability distribution function (PDF). Thus, we fit the flat Λ CDM model with the Kelly method (Kelly, 2007) using \mathcal{L}_{new} and considering these cases: H_0 fixed and Ω_M free, Ω_M fixed and H_0 free, and both parameters free. We impose wide uniform priors $0 \leq \Omega_M \leq 1$ and $50 \text{ km s}^{-1} \text{ Mpc}^{-1} \leq H_0 \leq 100 \text{ km s}^{-1} \text{ Mpc}^{-1}$ to guarantee that the parameter's space is explored in all physical regions. With the uninformative priors there is no difference on this approach and the Expectation Maximization algorithm used for the Maximum Likelihood Estimation (Dempster et al., 1977). We then repeat the fit with \mathcal{L}_{Gauss} , thus comparing the outcomes. Further, we test how the cosmological constraints vary if we change the assumptions on the fixed parameter in the cases of one free parameter. We consider $\Omega_M = 0.30$ and $\Omega_M = 0.34$, respectively from Scolnic et al. (2018) and Brout et al. (2022) for a flat

Λ CDM model when considering only SNe Ia with both statistical and systematic uncertainties, as in this work. We investigate $H_0 = 73.04 \text{ km s}^{-1} \text{ Mpc}^{-1}$ from Riess et al. (2022), and $H_0 = 70 \text{ km s}^{-1} \text{ Mpc}^{-1}$ based on Scolnic et al. (2018) and chosen arbitrarily (Cao et al., 2021; Abdalla et al., 2022).

We also compare our H_0 with the ones from *Pantheon* (P), *Pantheon +* ($P+$), and the CMB, by computing the z-score (ζ), a method to evaluate the statistical distance between a value and its reference value. ζ is defined as $\zeta = |H_{0,i} - H_{0,our}| / \sqrt{\sigma_{H_{0,i}}^2 + \sigma_{H_{0,our}}^2}$ where i is one of the three H_0 reference values with its 1σ uncertainty. $H_{0,our}$ and $\sigma_{H_{0,our}}$ are the H_0 and its 1σ error obtained in our computations. In Table 2 ζ_{CMB} is calculated referred to $H_0 = 67.4 \pm 0.5 \text{ km s}^{-1} \text{ Mpc}^{-1}$, ζ_P compared to $H_0 = 70.00 \pm 0.13 \text{ km s}^{-1} \text{ Mpc}^{-1}$, and ζ_{P+} with respect to $H_0 = 73.04 \pm 1.04 \text{ km s}^{-1} \text{ Mpc}^{-1}$. The parameter ζ helps to quantify the discrepancy between the H_0 values obtained in our analyses and the ones assumed as references. Additionally, we use the ζ parameter also to compare the values of Ω_M and H_0 obtained with \mathcal{L}_{new} and \mathcal{L}_{Gauss} for both *Pantheon* and *Pantheon +* samples. Following the previous definition of ζ , we define $\zeta_{\mathcal{L},\Omega_M}$ and $\zeta_{\mathcal{L},H_0}$ as $\zeta_{\mathcal{L},\Omega_M} = |\Omega_{M,\mathcal{L}_{new}} - \Omega_{M,\mathcal{L}_{Gauss}}| / \sqrt{\sigma_{\Omega_{M,\mathcal{L}_{new}}}^2 + \sigma_{\Omega_{M,\mathcal{L}_{Gauss}}}^2}$ and $\zeta_{\mathcal{L},H_0} = |H_{0,\mathcal{L}_{new}} - H_{0,\mathcal{L}_{Gauss}}| / \sqrt{\sigma_{H_{0,\mathcal{L}_{new}}}^2 + \sigma_{H_{0,\mathcal{L}_{Gauss}}}^2}$, where the subscripts \mathcal{L}_{new} and \mathcal{L}_{Gauss} refer to the specific likelihood used to fit the cosmological parameters. The obtained $\zeta_{\mathcal{L},\Omega_M}$ and $\zeta_{\mathcal{L},H_0}$ are reported in Table 3 for each case analysed in this work.

Since the z-score allows us to quantitatively compare two results and evaluate their relative compatibility or discrepancy, we use this parameter also to test if the cosmological results obtained in all cases by employing Equation 2 are consistent with the ones derived by applying Equation 3. Thus, we define ζ_{Ω_M} and ζ_{H_0} as $\zeta_{\Omega_M} = |\Omega_{M,2} - \Omega_{M,3}| / \sqrt{\sigma_{\Omega_{M,2}}^2 + \sigma_{\Omega_{M,3}}^2}$ and $\zeta_{H_0} = |H_{0,2} - H_{0,3}| / \sqrt{\sigma_{H_{0,2}}^2 + \sigma_{H_{0,3}}^2}$, where the subscripts 2 and 3 refer to the Equation 2 and 3 used respectively to fit the cosmological parameters. The obtained ζ_{Ω_M} and ζ_{H_0} are reported in Table 4 for each case studied in this work. More specifically, in this table we present the sample (i.e. *Pantheon* or *Pantheon +*) in the first column, the cosmological case considered (i.e. if H_0 is fixed to 70 or 73.04, if Ω_M is fixed to 0.3 or 0.34, or if both Ω_M and H_0 are free to vary) in the second column, and the values of ζ_{Ω_M} and ζ_{H_0} in the other columns. The table is also divided to distinguish the two different likelihoods adopted. The symbol “-” refers to the cases in which H_0 is fixed and thus ζ_{H_0} cannot be computed and the cases in which Ω_M is fixed and, as a consequence, ζ_{Ω_M} cannot be calculated.

3. Results

3.1. Gaussianity tests results

Both SNe Ia samples do not pass neither the Anderson-Darling nor the Shapiro-Wilk tests. Thus, the null hypothesis that $\Delta\mu_{norm}$ comes from a Gaussian distribution should be rejected. The Anderson-Darling test rejects the Gaussianity

hypothesis to a significance level $> 15\%$. This rejection is confirmed by the Shapiro-Wilk test as its p-value is $< 5\%$, the minimum value required to accept the null hypothesis. Given the limits of these methods, we compute the skewness and kurtosis of the $\Delta\mu$ normalized distributions. The *Pantheon* sample has skewness = -0.08 and kurtosis = 0.44 corresponding to an excess of the tail on the left, while the *Pantheon +* presents the skewness = -0.50 and more prominent tails with kurtosis = 3.9 (see Fig. 1). As also visible from the right panel of Fig. 1, the skewness of *Pantheon +* is larger than the one of *Pantheon*. Neither of the samples passes the skewness, kurtosis and “skewness+kurtosis” tests. As anticipated in Sect. 2.2, we also verify that the results of all the normality tests are independent on the assumed cosmology and they do not change when using Equation 3 in place of Equation 2. All these independent normality tests result in coherent and consistent results guaranteeing the common outcome and strongly proving that the $\Delta\mu_{norm}$ of SNe Ia is not normally distributed, neither for the *Pantheon* nor for the *Pantheon +* sample. The Gaussianity implicit assumption for SNe Ia $\Delta\mu_{norm}$ is not statistically legitimated and it should be checked for each SNe Ia sample used.

3.2. New best-fit distributions

Thus, the $\Delta\mu_{norm}$ distributions are not well-fitted by the Gaussian PDF, defined as:

$$\text{PDF}_{\text{Gaussian}} = \frac{1}{\sqrt{2\pi}\sigma} e^{-\frac{1}{2}\left(\frac{x-\hat{x}}{\sigma}\right)^2} = \frac{1}{\sqrt{2\pi}\sigma} e^{-\frac{1}{2}\chi^2} \quad (6)$$

where \hat{x} is the mean, σ is the standard deviation, $x - \hat{x} = \Delta\mu$ and χ^2 is the same defined in Eq. (4). Hence, we fit the $\Delta\mu$ histograms (see Sec. 2.2) obtaining as the best fit for the *Pantheon* sample a logistic distribution, with the following PDF

$$\text{PDF}_{\text{logistic}} = \frac{e^{-\frac{(x-\hat{x})}{s}}}{s \left(1 + e^{-\frac{(x-\hat{x})}{s}}\right)^2} = \frac{e^{-\chi'^2}}{s \left(1 + e^{-\chi'^2}\right)^2} \quad (7)$$

where s is scale and the variance σ^2 is $\sigma^2 = (s^2\pi^2)/3$. As for the Gaussian PDF, we consider the whole covariance matrix with both diagonal and non-diagonal components to account for all contributions to the uncertainty. Indeed, in the case of the logistic distribution, χ^2 is the same defined in Eq. (4) but in which the elements of C are multiplied by $3\sigma^2/\pi^2$. Hence, χ'^2 is defined as $\chi'^2 = \Delta\mu^T (3\sigma^2 C / \pi^2)^{-1} \Delta\mu$. Left panel of Fig. 1 shows the best-fit distributions normalized with the uncertainties on the singular SNe Ia of the logistic with $\hat{x} = -0.019$ and $s = 0.55$ (orange) and the Gaussian with $\hat{x} = 0.030$ and $\sigma = 0.99$ (green).

The same analysis is then repeated for the *Pantheon +* data. In this case, the distribution that best fits the histogram of $\Delta\mu_{norm}$ is a Student's t-distribution, for which the generalized PDF is

given by

$$\begin{aligned} \text{PDF}_{\text{student}} &= \frac{\Gamma\left(\frac{\nu+1}{2}\right)}{\sqrt{\nu\pi} s \Gamma\left(\frac{\nu}{2}\right)} \left[1 + \frac{((x-\hat{x})/s)^2}{\nu}\right]^{-\frac{\nu+1}{2}} \\ &= \frac{\Gamma\left(\frac{\nu+1}{2}\right)}{\sqrt{\nu\pi} s \Gamma\left(\frac{\nu}{2}\right)} \left[1 + \frac{\chi'^2}{\nu}\right]^{-\frac{\nu+1}{2}} \end{aligned} \quad (8)$$

where Γ is the gamma function, ν are the degrees of freedom, and $\sigma^2 = (s^2\nu)/(\nu-2)$. As explained for the logistic case, this relation between s and σ allows us to substitute C used in χ^2 of Eq. (4) for the Student's t. More specifically, $\chi'^2 = \Delta\mu^T [(\nu-1)\sigma^2 C / \nu]^{-1} \Delta\mu$. In our case, $x = \Delta\mu$ and $\hat{x} = 0$, as before. The best-fit distributions of the Student's t with $\hat{x} = 0.01$, $s = 0.20$, and $\nu = 4.2$ (orange) and the Gaussian with $\hat{x} = 0.018$ and $\sigma = 0.30$ (green) are shown in the middle panel of Fig. 1 where the distribution is normalized with the SNe Ia uncertainties (Eq. (6)). For the *Pantheon* and *Pantheon +* respectively, the logistic and the Student's t distributions better reproduce $\Delta\mu_{norm}$ in all the features (e.g. peak, central width, and tails) compared to the Gaussian PDF. We have also proved that these results remain the same if we apply Equation 3 instead of Equation 2 and if we change the cosmological assumption of a flat Λ CDM model with $\Omega_M = 0.3$ and $H_0 = 70 \text{ km s}^{-1} \text{ Mpc}^{-1}$, as already stated in Sect. 2.2. The first best-fit distribution for both *Pantheon* and *Pantheon +* samples is reported along with the other four that better fit the data in Table 1. As anticipated in Sect. 2.3, the most appropriate, namely the best-fit distributions, are ranked through the evaluation of the logarithm of the likelihood, BIC and AIC parameters, and the p-values of Pearson χ^2 and Cramer Von Mises tests. We have also proved that the logistic for the *Pantheon* and the Student-T distribution for the *Pantheon +* are favoured against the Gaussian distributions with the BIC. We used for comparison the table in Kass and Raftery (1995) to distinguish among the most favoured models. We have used the definition of $2\log_e(B_{10})$, where the Bayes factor $B_{10} = e^{(BIC_0 - BIC_1)/2}$ (Wagenmakers, 2007), B_0 is the reference model (the Gaussian), and B_1 is the alternative model (either the logistic or the T-student distribution). Thus, $2\log_e(B_{10}) = BIC_0 - BIC_1 = \Delta_{BIC}$. We found $\Delta_{BIC, \text{Pantheon}} = 7$ showing strong evidence for the Logistic against the Gaussian distribution, and $\Delta_{BIC, \text{Pantheon+}} = 150$ showing very strong evidence for the T-Student against the Gaussian for the Pantheon+. By definition, for $6 \leq \Delta_{BIC} \leq 10$ the evidence against the null hypothesis (the Gaussian being the favorite the model) is strong, when $\Delta_{BIC} > 10$ the evidence against the null hypothesis is very strong. However, we would like to stress that the BIC works under the assumption that the variables are independent. Since SNe Ia are correlated, the BIC test may less trustworthy. Thus, we prefer to apply the AIC, since it does not include the number of SNe Ia. Indeed, it is also worth noting that some of the SNe Ia are repeated in the sample, since they belong to different survey. When computing the AIC, we still find that the logistic distribution is favored against the Gaussian since the AIC of the logistic is lower than the one of the Gaussian of a factor 8. Moreover, also the Student-T is favored against the Gaussian, with an AIC parameter that is

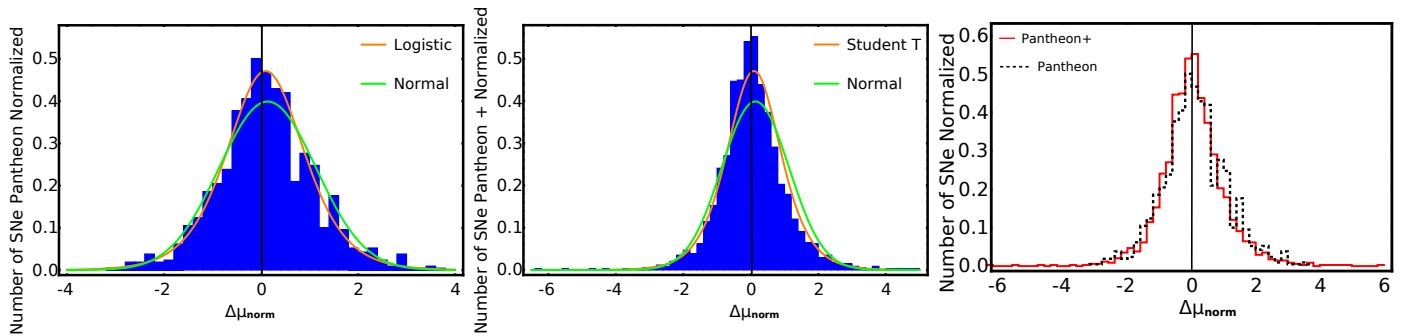


Figure 1: Normalized $\Delta\mu_{norm}$ histogram, defined as $\Delta\mu_{norm} = C^{-1/2} \Delta\mu$, for the 1048 SNe Ia in *Pantheon* (left panel) and the 1701 SNe Ia in *Pantheon +* (middle panel). The green curve is the best-fit Gaussian distribution, while the orange curves are the best-fit logistic (left panel) and Student’s t (middle panel) distributions. Right panel shows the superimposition of the *Pantheon* and *Pantheon +* distributions. In all panels the vertical black line marks the zero line.

lower of a factor 150 compared to the one of the Gaussian distribution. However, we would like to take a further step in the discussion. The number of actual SNe Ia observed is smaller than the total number of SNe Ia either in the *Pantheon* or in the *Pantheon+* sample, thus the BIC criterion could be corrected for a smaller number of SNe Ia. When the number of parameters is different, e.g. the T-student has 3 parameters instead of two of the Gaussian, the difference of the BIC would be even larger, thus showing the reliability of these likelihoods against the Gaussian one. Although there may be more refined criteria for this study, the analysis of this comparison would require a more complex statistical study, which goes far beyond the scope of the paper. Moreover, we have proved the goodness of the fits with the Anderson-Darling one-sample test. The results yield a probability value that the fit is not randomly drawn, $p = 0.97$ for the *Pantheon* sample for the logistic distribution, and $p = 0.88$ for the *Pantheon +* for the Student-T distribution. For visual clarity, right panel of Fig. 1 shows the comparison between the normalized residuals $\Delta\mu_{norm}$ of *Pantheon* (in dashed gray) and *Pantheon+* (in continuous red). This superimposition clearly proves that the *Pantheon+* distribution is more peaked and presents heavier tails compared to *Pantheon*. This difference stems from the sources present in *Pantheon+* and not in *Pantheon*. Furthermore, this discrepancy causes the difference between the two corresponding best-fit distributions, namely the change from the logistic distribution for the *Pantheon* SNe Ia to the Student-T for the *Pantheon+*. Although our analysis is statistically reliable, we here stress that this reasoning is valid if the distributions of Fig. 1 are derived from a perfect sample and modeling of selection effects. If, however, there are problems with some of these sources, such as bad background subtraction, cosmic ray hit etc. this surely can impact the distribution, but a deep analysis of these sources is far beyond the scope of the current analysis. We here assume that the *Pantheon* and *Pantheon+* samples are trustworthy sources.

3.3. Cosmology with the Gaussian and new likelihoods

We here comment and interpret our cosmological results. As shown in Table 4, the values obtained for Ω_M and H_0 when applying Equation 2 and Equation 3 are completely consistent

within 0.3σ , thus proving that our results are robust and independent on the specific formula used to compute the theoretical distance moduli. Hence, the following considerations are valid for both cases.

Using \mathcal{L}_{new} , we fit the flat Λ CDM model on the *Pantheon* and *Pantheon+* samples (see Section 2.3). Table 2 reports the best-fit values with 68% confidence level. Left panel of Fig. 2 show the corner plots (with blue contours) from the logistic likelihood ($\mathcal{L}_{logistic}$), while right panel of Fig. 2 the ones from the Student’s t likelihood ($\mathcal{L}_{Student}$) in blue. For the Student’s t, we treat the degrees of freedom ν as a free parameter by imposing a wide uniform prior in the range $0 < \nu < 6$. In principle, we could consider it as a free parameter or we could fix it a priori and fit only the cosmological parameters. To investigate this choice, we have tested both approaches. This analysis has shown that, if we fix ν to its best-fit value $\nu = 4.2$ obtained from the fit of the histogram of $\Delta\mu_{norm}$ for *Pantheon+* in the middle panel of Fig. 1 (see Section 3.1), the values of Ω_M and H_0 obtained are compatible within 0.2σ with the ones derived when ν is free to vary. Thus, this choice does not impact our cosmological results. Moreover, ν does not manifest any correlation with the cosmological free parameters, as can be seen in right panel of Fig. 2, hence the estimates of Ω_M and H_0 are independent on the treatment of ν , which is if we fix it or leave it free. Thus, we have decided to apply the more general approach of using ν as a free parameter, which also allows us to perform a more accurate analysis, without the need for knowing the value of this parameter a priori. The results of the fit of the flat Λ CDM model with \mathcal{L}_{Gauss} are in Table 2 and in red in Fig. 2.

Considering the *Pantheon* sample, the cosmological parameters obtained with \mathcal{L}_{Gauss} and $\mathcal{L}_{logistic}$ are compatible in 1σ , except for Ω_M when $H_0 = 73.04 \text{ km s}^{-1} \text{ Mpc}^{-1}$, that shows a $2 - 3\sigma$ discrepancy. Concerning the uncertainties, $\mathcal{L}_{logistic}$ shows significantly tighter constraints when both Ω_M and H_0 are free parameters: the errors on Ω_M and H_0 are reduced by 43% (from 0.021 to 0.012) and 41% (from 0.34 to 0.20), respectively. Same conclusions are drawn for the *Pantheon+*. The only difference is that the 3σ discrepancy in Ω_M emerges when $H_0 = 70 \text{ km s}^{-1} \text{ Mpc}^{-1}$. This can be ascribed to the $H_0 = 73.04 \text{ km s}^{-1} \text{ Mpc}^{-1}$ assumed for *Pantheon+*. The use

<i>Pantheon</i>	Distributions	Log Likelihood	AIC	BIC	Pearson χ^2	Cramer Von Mises
	Logistic	0.54	51.5	-7555	0.84	0.71
	Gaussian	0.53	53.3	-7030	0.006	0.006
	Student's t	0.53	47.6	-6820	0.02	0.0001
	Weibull	0.52	59.7	-6577	0.001	0.0001
	Laplace	0.51	73.2	-6764	2×10^{-5}	1×10^{-6}
<i>Pantheon +</i>						
	Student's t	0.33	176.1	-16890	0.08	0.06
	Logistic	0.33	218.6	-15201	0.08	0.6
	Laplace	0.30	178.9	-12943	3×10^{-10}	0.003
	Gaussian	0.28	334.3	-12567	8×10^{-23}	9×10^{-10}
	Cauchy	0.20	125.5	-12005	7×10^{-53}	2×10^{-5}

Table 1: First five best-fit distributions of $\Delta\mu_{norm}$ for both *Pantheon* and *Pantheon +* samples. The columns next to each distribution show the values of the following computed parameters: logarithm of the likelihood, AIC, BIC, p-value of Pearson χ^2 test, and p-value of the Cramer Von Mises test (see also Sect. 2.3).

of $\mathcal{L}_{Student}$ reduces the errors on Ω_M and H_0 , when both are free parameters, by 42% (from 0.019 to 0.011) and 33% (from 0.24 to 0.16), respectively. Further, Planck Collaboration et al. (2020) reported $\Omega_M = 0.315 \pm 0.007$. Thus, the discrepancy with the values in Table 2, when Ω_M and H_0 are free, increases using \mathcal{L}_{new} due to the reduced errors. Quantitatively, $\mathcal{L}_{logistic}$ shows a 2σ discrepancy compared to 1σ of \mathcal{L}_{Gauss} , while $\mathcal{L}_{Student}$ increases the discrepancy from 2 to 3 σ .

The current study highlights differences in the uncertainties of the Hubble constant (H_0) as compared to the findings reported in previous works by Riess et al. (2019) and Riess et al. (2022), which focused on the *Pantheon* and *Pantheon+* data sets. As already detailed in Bargiacchi et al. (2023), these variations in uncertainties are attributed to distinct approaches used in determining H_0 in the different studies. Specifically, Riess et al. (2019) and Riess et al. (2022) employed various methods, such as analyzing Cepheids in SNe Ia hosts, Cepheids as anchors or non-SNe Ia hosts, SNe Ia in Cepheids hosts, external constraints, and SNe Ia in the Hubble flow. In their analyses, they also considered free parameters in the fit, including $5 \log H_0$, from which H_0 and its uncertainty were derived. Additionally, a contribution to the systematic uncertainty from different analysis variants was included. In Riess et al. (2022), the value of H_0 was used, along with its corresponding M parameter, to calculate the distance moduli and their uncertainties for the *Pantheon+* release. In contrast, the *Pantheon* release assumed $H_0 = 70$ when providing distance moduli. In this present study, a distinct approach is taken. The entire SNe Ia sample (1048 sources for *Pantheon* and 1701 sources for *Pantheon+*) is considered, and direct fitting of the distance moduli and their uncertainties, is performed contrary to the approach in Riess in which the fit is calibrated with 42 Cepheids. In our approach, the values of M are fixed in the fitting process, to the corresponding values of the distance moduli to either $H_0 = 70$ or $H_0 = 73.04$, depending on the data set (*Pantheon* or *Pantheon +*), respectively. As a result of this approach, the uncertainties on H_0 obtained in the current study are significantly reduced compared to those reported in Riess et al. (2019) and Riess et al. (2022).

Additional interesting trends are revealed when comparing the cosmological results from the two SNe Ia samples, in-

dependently on the \mathcal{L} considered. With *Pantheon*, we recover $\Omega_M = 0.3$ and $H_0 = 70 \text{ km s}^{-1} \text{ Mpc}^{-1}$, as in Scolnic et al. (2018), except when assuming $\Omega_M = 0.34$ and $H_0 = 73.04 \text{ km s}^{-1} \text{ Mpc}^{-1}$. Conversely, with *Pantheon+*, we recover $\Omega_M = 0.35$ and $H_0 = 73 \text{ km s}^{-1} \text{ Mpc}^{-1}$ as in Brout et al. (2022) and Riess et al. (2022), except when fixing $H_0 = 70 \text{ km s}^{-1} \text{ Mpc}^{-1}$. The significant shifts in Ω_M show how strongly the choice of M (and thus H_0) used to compute μ affects the cosmological results. We have performed reverse engineering reasoning: we have used the same distance moduli provided by Scolnic et al. (2018) and Brout et al. (2022) by using the covariance matrix which include both statistics and systematic uncertainties. We have used the same assumption on H_0 used in Scolnic et al. (2018) and in Brout et al. (2022). Thus, if there was no hidden selection biases or redshift evolution at play, we should have recovered the values of the assumption for Ω_M . However, when we fix this value of H_0 we have a varying Ω_M as an inherent evidence of an evolving trend in H_0 already extensively discussed in Dainotti et al. (2021, 2022a) for which Schiavone et al. (2023) have further provided a theoretical explanation. This trend of Ω_M (also discussed in Colgáin et al. (2022b,a)) can be either the consequence that we are forcing the value of H_0 to be fixed while an evolving trend is present in the data or that there is an inherent crisis of the Λ CDM model that brings to an evolving trend of Ω_M . Another possibility is that there are selection biases or evolutionary effects at play which are still unclear. The difference in the trend of Ω_M and H_0 could be due to the fact that in the local Universe we do not see a dependence on Ω_M and H_0 which instead is revealed at high- z . Anyhow, regardless of the physical meaning and the explanation such a trend is revealed in the data and is important to highlight the impact associated with the quantification of the H_0 tension. The evolving trend of H_0 is shown also in Jia et al. (2022) with $H(z)$ and additional data samples for the SNe Ia.

Additionally, we compute ζ (see Sec. 2.3) for each cosmological computation (Table 2). The high ζ_P values (~ 20) when calculated for the *Pantheon+* sample may depend on the smaller error on the reference value $H_0 = 70.00 \pm 0.13 \text{ km s}^{-1} \text{ Mpc}^{-1}$ compared to the errors of the reference values pertinent to ζ_{CMB} and ζ_{P+} . ζ_{P+} is always ~ 3 when computed for *Pantheon*;

ζ_{CMB} is higher for *Pantheon+* ($\zeta_{CMB} \sim 12$) than *Pantheon* ($\zeta_{CMB} \sim 5$) as the H_0 value in Riess et al. (2022) is more discrepant from the one derived from CMB compared to the H_0 in Scolnic et al. (2018). Concerning the ζ reported in Table 3 and computed to compare the cosmological parameters obtained with \mathcal{L}_{new} and \mathcal{L}_{Gauss} , we notice that the highest values are the ones obtained when H_0 is fixed and Ω_M is free to vary. Indeed, for *Pantheon* the maximum value is $\zeta_{\mathcal{L},\Omega_M} = 3.1$, obtained when $H_0 = 73.04 \text{ km s}^{-1} \text{ Mpc}^{-1}$, while for *Pantheon+* we obtain the maximum value of $\zeta_{\mathcal{L},\Omega_M} = 3.7$ when $H_0 = 70 \text{ km s}^{-1} \text{ Mpc}^{-1}$. This result is expected since *Pantheon* SNe Ia favour $H_0 = 70 \text{ km s}^{-1} \text{ Mpc}^{-1}$, while *Pantheon+* prefers $H_0 = 73.04 \text{ km s}^{-1} \text{ Mpc}^{-1}$. The reason why we do not obtain high values also of $\zeta_{\mathcal{L},H_0}$ when Ω_M is fixed is that the uncertainties on H_0 are larger than the ones on Ω_M (see Table 2) and hence the denominator in the definition of the $\zeta_{\mathcal{L},H_0}$ is larger than the one of $\zeta_{\mathcal{L},\Omega_M}$ making $\zeta_{\mathcal{L},H_0}$ smaller than $\zeta_{\mathcal{L},\Omega_M}$. The fact that the values of ζ reported in Table 3 are always < 1 , except for the two cases discussed above, shows that the best-fit values of Ω_M and H_0 obtained with the new best-fit likelihoods and the Gaussian likelihood are compatible, as already stressed above. Nonetheless, the crucial point is that the use of \mathcal{L}_{new} significantly reduces the uncertainties on these cosmological parameters compared to \mathcal{L}_{Gauss} . Indeed, $\mathcal{L}_{logistic}$ reduces the uncertainties on Ω_M and H_0 up to 43% (from 0.021 to 0.012) and 41% (from 0.34 to 0.20), respectively, while $\mathcal{L}_{Student}$ reduces the error on Ω_M and H_0 up to 42% (from 0.019 to 0.011) and 33% (from 0.24 to 0.16), respectively.

4. Conclusions

We have investigated the Gaussianity assumption on the distance moduli μ of *Pantheon* (Scolnic et al., 2018) and *Pantheon+* (Scolnic et al., 2022) of SNe Ia, including both statistical and systematic uncertainties. We show that this assumption, usually implicitly assumed, is not fulfilled via the Anderson-Darling and Shapiro-Wilk normality tests, and the skewness, kurtosis, and “skewness+kurtosis” tests. We have computed the distribution of the normalized, via the C matrix, difference between the μ observed and the μ expected under the assumption of an underlying cosmological model. We have assumed a flat Λ CDM model with $\Omega_M = 0.3$ and $H_0 = 70 \text{ km s}^{-1} \text{ Mpc}^{-1}$, but we have checked our results against this assumption testing also other specific values. We have also proved that our results do not change if we compute the theoretical μ with the general Eq. 3 in place of the Eq. 2 from Kenworthy et al. (2019), which is more suitable for low redshifts. We have used several statistical methods to verify if $\Delta\mu_{norm}$ is normally distributed. Independent and complementary approaches are crucial to guarantee reliable results, leveraging on the advantages and minimizing the limits of each method. Both SNe Ia samples fail all of these tests revealing a non-Gaussian $\Delta\mu_{norm}$ distribution. Consequently, the traditional practise of constraining cosmological parameters with SNe Ia by maximizing the Gaussian distance moduli likelihood is not appropriate, as it is not grounded on a statistical base. We have then unveiled the hidden underlying distributions of $\Delta\mu_{norm}$, by using two different built-in functions in Wolfram

Mathematica and Python, which employ several statistical tests (see Sect. 2.3) to compare among numerous distributions. We notice that the best-fit distributions are the Student’s t and the logistic for the *Pantheon* and *Pantheon+*, respectively, among all the distributions we tried. The logistic and the Student’s t distributions are the ones that best fit *Pantheon* and *Pantheon+*, respectively (see Fig. 1). This is clearly visualized in Fig. 1, where the corresponding best-fit curves (in orange) better reproduce the $\Delta\mu$ histograms of the two SNe Ia samples compared to the Gaussian best-fit curve (in green). This result is also visible from Table 1, in which the first five best-fitting distributions for both *Pantheon* and *Pantheon+* are shown along with the corresponding evaluated statistical tests. Indeed, the logistic and Student’s t distributions, respectively for *Pantheon* and *Pantheon+*, are the favored ones according to the values of the logarithm of the likelihood, BIC, AIC, and p-values of Pearson χ^2 and Cramer Von Mises tests. Following these results, we have fitted the flat Λ CDM model using both $\mathcal{L}_{Gaussian}$ and the logistic ($\mathcal{L}_{logistic}$) and Student’s t ($\mathcal{L}_{Student}$) likelihoods, for the *Pantheon* and the *Pantheon+* samples, respectively.

Here, we summarize the main points. The $\mathcal{L}_{logistic}$ and $\mathcal{L}_{Student}$, used to fit respectively the *Pantheon* and *Pantheon+* samples, with a flat Λ CDM model with both Ω_M and H_0 free parameters, significantly reduce the uncertainties on these parameters. $\mathcal{L}_{logistic}$ reduces the uncertainties on Ω_M and H_0 by 43% (from 0.021 to 0.012) and 41% (from 0.34 to 0.20), respectively, while $\mathcal{L}_{Student}$ reduces the error on Ω_M and H_0 by 42% (from 0.019 to 0.011) and 33% (from 0.24 to 0.16), respectively. Our results steadily demonstrate that these new distributions perform better on the data compared to the Gaussian. In addition, we have demonstrated that choosing the actual distribution for each SNe Ia sample is key to substantially improving the constraints on cosmological parameters.

In conclusion, we show that $\Delta\mu_{norm}$ of *Pantheon* and *Pantheon+* does not verify the Gaussianity assumption. This result has a significant repercussion on the SNe Ia cosmology, the approach implicitly assumed in SNe Ia cosmology, and future SNe Ia collections for which the Gaussianity assumption will have to be carefully inspected. In an era in which the cosmological debate is focused on tensions in the cosmological parameters, the reduction of $\sim 40\%$ in Ω_M and H_0 represents a breakthrough to constrain cosmological parameters more precisely, thus shedding light on the effective extent of these tensions.

Acknowledgements

This study uses data from <https://github.com/dscolnic/Pantheon> and <https://github.com/PantheonPlusSH0ES>. GB acknowledges Scuola Superiore Meridionale, for supporting her visit at NAOJ, Division of Science. GB thanks the Division of Science for being hosted on campus. MGD acknowledges NAOJ. We thank M. Ghodsi Yengejeh for the work on the right panel of Fig. 1.

Authors contributions

Conceptualization: MB, MGD, GB, SN

$\mathcal{L}_{logistic}$						\mathcal{L}_{Gauss}					
<i>Pantheon</i>	H_0	Ω_M		ζ_{CMB}	ζ_P	ζ_{P+}	H_0	Ω_M	ζ_{CMB}	ζ_P	ζ_{P+}
	70	0.295 ± 0.007					70	0.300 ± 0.009			
	73.04	0.173 ± 0.006					73.04	0.144 ± 0.007			
	70.00 ± 0.13	0.3		5.73	0	2.90	70.00 ± 0.13	0.3	5.73	0	2.90
	69.47 ± 0.12	0.34		4.73	2.96	3.41	69.43 ± 0.14	0.34	4.60	2.98	3.44
	70.21 ± 0.20	0.285 ± 0.012		5.89	0.88	2.67	69.99 ± 0.34	0.300 ± 0.021	4.88	0.03	2.79
$\mathcal{L}_{Student}$						\mathcal{L}_{Gauss}					
<i>Pantheon+</i>	H_0	Ω_M	ν	ζ_{CMB}	ζ_P	ζ_{P+}	H_0	Ω_M	ζ_{CMB}	ζ_P	ζ_{P+}
	70	0.532 ± 0.010	3.35 ± 0.07				70	0.587 ± 0.011			
	73.04	0.345 ± 0.007	3.05 ± 0.06				73.04	0.349 ± 0.010			
	73.50 ± 0.11	0.3	3.07 ± 0.06	12.62	20.55	0.44	73.51 ± 0.12	0.3	12.58	19.84	0.45
	73.06 ± 0.11	0.34	3.05 ± 0.06	11.76	17.97	0.02	73.06 ± 0.13	0.34	11.65	16.64	0.02
	72.93 ± 0.16	0.352 ± 0.011	3.06 ± 0.06	11.22	14.21	0.10	72.85 ± 0.24	0.361 ± 0.019	10.48	10.44	0.18

Table 2: Best-fit values with 1σ uncertainties for *Pantheon* and *Pantheon+*, for all cosmological cases and \mathcal{L} . Fixed cosmological parameters are in bold. H_0 is in $\text{km s}^{-1} \text{Mpc}^{-1}$.

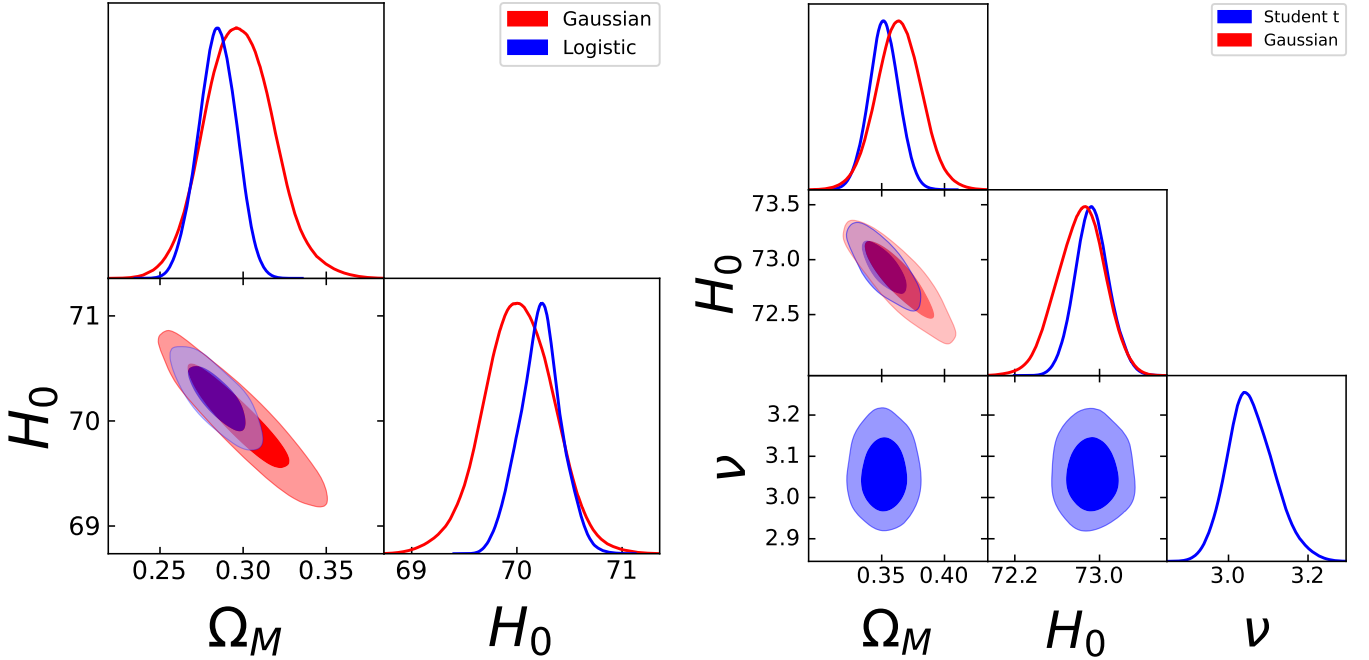


Figure 2: Fit of the flat Λ CDM model with Ω_M and H_0 free parameters. Left panel shows the results for *Pantheon* SNe Ia with both \mathcal{L}_{Gauss} and $\mathcal{L}_{logistic}$ as in the legend. Right panel shows the contours for the *Pantheon+* sample with both \mathcal{L}_{Gauss} and $\mathcal{L}_{Student}$ as illustrated in the legend.

$\mathcal{L}_{logistic}$ vs \mathcal{L}_{Gauss}			
<i>Pantheon</i>	Case	$\zeta_{\mathcal{L},\Omega_M}$	$\zeta_{\mathcal{L},H_0}$
	$H_0 = 70$	0.4	-
	$H_0 = 73.04$	3.1	-
	$\Omega_M = 0.3$	-	0
	$\Omega_M = 0.34$	-	0.2
	Ω_M, H_0 free	0.6	0.07
$\mathcal{L}_{Student}$ vs \mathcal{L}_{Gauss}			
<i>Pantheon +</i>	Case	$\zeta_{\mathcal{L},\Omega_M}$	$\zeta_{\mathcal{L},H_0}$
	$H_0 = 70$	3.7	-
	$H_0 = 73.04$	0.3	-
	$\Omega_M = 0.3$	-	0.06
	$\Omega_M = 0.34$	-	0
	Ω_M, H_0 free	0.4	0.3

Table 3: Computed values of $\zeta_{\mathcal{L},\Omega_M}$ and $\zeta_{\mathcal{L},H_0}$, as described in Section 2.3. The first column reports the sample studied, the second one the cosmological case considered, and the other ones the values of $\zeta_{\mathcal{L},\Omega_M}$ and $\zeta_{\mathcal{L},H_0}$. H_0 is in units of $\text{km s}^{-1} \text{Mpc}^{-1}$. We use the notation “-” to indicate the cases in which the z-score cannot be computed since the cosmological parameter is fixed and not fitted in the cosmological analysis.

$\mathcal{L}_{logistic}$		\mathcal{L}_{Gauss}			
<i>Pantheon</i>	Case	ζ_{Ω_M}	ζ_{H_0}	ζ_{Ω_M}	ζ_{H_0}
	$H_0 = 70$	0.2	-	0.2	-
	$H_0 = 73.04$	0	-	0.1	-
	$\Omega_M = 0.3$	-	0.1	-	0.3
	$\Omega_M = 0.34$	-	0.1	-	0.2
	Ω_M, H_0 free	0.1	0.07	0.06	0
$\mathcal{L}_{Student}$		\mathcal{L}_{Gauss}			
<i>Pantheon +</i>	Case	ζ_{Ω_M}	ζ_{H_0}	ζ_{Ω_M}	ζ_{H_0}
	$H_0 = 70$	0.1	-	0.1	-
	$H_0 = 73.04$	0.1	-	0.07	-
	$\Omega_M = 0.3$	-	0	-	0.06
	$\Omega_M = 0.34$	-	0.06	-	0
	Ω_M, H_0 free	0.2	0.04	0.04	0.03

Table 4: Computed values of ζ_{Ω_M} and ζ_{H_0} , as described in Section 2.3, for both the new likelihoods and the Gaussian likelihood. The first column reports the sample studied, the second one the cosmological case considered, and the other ones the values of ζ_{Ω_M} and ζ_{H_0} . H_0 is in units of $\text{km s}^{-1} \text{Mpc}^{-1}$. We use the notation “-” to indicate the cases in which the z-score cannot be computed since the cosmological parameter is fixed and not fitted in the cosmological analysis.

Data curation: GB
 Formal Analysis: MGD, GB
 Funding acquisition: MGD, MB
 Investigation: GB, MGD
 Methodology: MGD
 Software: GB, MGD
 Supervision: MGD
 Writing – original draft: GB, MGD
 Writing – review & editing: MGD, GB, MB, SC, SN

Conflicts of interest

The authors declare no conflict of interest.

Data Availability

This study uses data from <https://github.com/dscolnic/Pantheon> and <https://github.com/PantheonPlusSH0ES>.

Appendix A. Tests with mock samples

To further test the reliability of our results we have generated mock data for the redshift, the distance moduli, μ , assuming a given cosmology, and the uncertainties on the distance moduli for both Pantheon (1048 mock data) and Pantheon+ (1701 mock data) samples by extracting random values from their actual distributions. We here show that the observed redshift distribution for the Pantheon sample is a Mixture Gaussian distribution between a Normal distribution with mean=0.2 and standard deviation $\sigma = 0.13$, and a Γ distribution with the shape parameter 6.3 and a scale of 0.1, see the upper left panel of Fig. A.3. For the Pantheon+, we still have a Gaussian Mixture distribution between a Normal with mean=0.12 and $\sigma = 0.11$ and a log-Normal with a mean of -0.66 and $\sigma = 0.38$, see the upper right panel of Fig. A.3.

We have then checked that the distribution of the mock sample for $\Delta\mu_{norm}$ for the Pantheon sample obtained from the mock redshift distribution resembling the observed sample is still a logistic distribution and for the Pantheon+ sample is still a Student’s T distribution. The lower left and right panels of Fig. A.3 show the best-fit distributions of $\Delta\mu_{norm}$ superimposed in orange to the differential distributions for the Pantheon and Pantheon+ samples, respectively. As a comparison for both panels we have also shown the corresponding Gaussian fit in green in both panels.

We have then computed the μ with the theoretical formula in Eq. (2) assuming a given cosmological model in the flat Λ CDM model. Specifically, we have tested three cases: $\Omega_M = 0.3$ and $H_0 = 70 \text{ km s}^{-1} \text{Mpc}^{-1}$, $\Omega_M = 0.8$ and $H_0 = 65 \text{ km s}^{-1} \text{Mpc}^{-1}$, and $\Omega_M = 0.1$ and $H_0 = 80 \text{ km s}^{-1} \text{Mpc}^{-1}$. We have fitted the mock data leaving together Ω_M and H_0 free to vary both with the Gaussian and the Logistic likelihood, see the upper and lower panels of Fig. A.4, respectively, for Pantheon SNe Ia. We have fitted the Gaussian and the Student’s T likelihoods for Pantheon+ SNe Ia again leaving both Ω_M and H_0 free to vary,

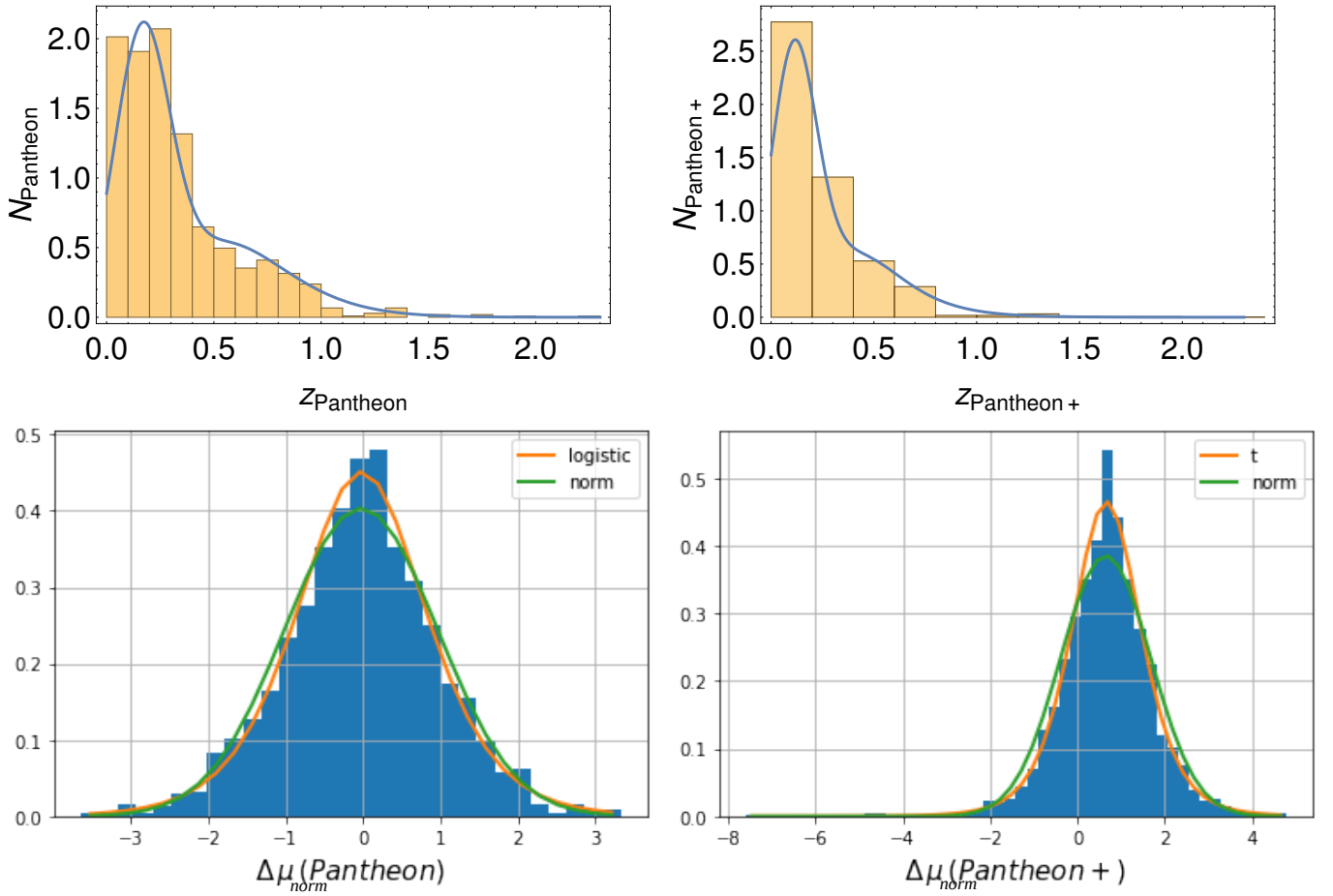


Figure A.3: Upper panels: Redshift distributions for mock samples built from the 1048 *Pantheon* SNe Ia (left panel) and the 1701 *Pantheon +* SNe Ia (right panel). The blue curves are the corresponding best-fit mixture distributions. Lower panels: Normalized $\Delta\mu_{norm}$ histogram for the mock samples of the 1048 SNe Ia in *Pantheon* (left panel) and the 1701 SNe Ia in *Pantheon +* (right panel) obtained assuming a flat Λ CDM model with $\Omega_M = 0.3$ and $H_0 = 70 \text{ km s}^{-1} \text{ Mpc}^{-1}$. The green curve is the best-fit Gaussian distribution, while the orange curves are the best-fit logistic (left panel) and Student's t (right panel) distributions.

see the upper and lower panels of Fig. A.5, respectively. As it is shown in the figures, all results with the observed distributions are confirmed by the ones obtained with the mock samples.

References

- Abdalla, E., Abellán, G.F., Aboubrahim, A., Agnello, A., Akarsu, Ö., Akrami, Y., Alestas, G., Aloni, D., Amendola, L., Anchordoqui, L.A., Anderson, R.I., Arendse, N., Asgari, M., Ballardini, M., Barger, V., Basilakos, S., Batista, R.C., Battistelli, E.S., Batty, R., Benetti, M., Benisty, D., Berlin, A., de Bernardis, P., Berti, E., Bиденко, B., Birrer, S., Blakeslee, J.P., Boddy, K.K., Bom, C.R., Bonilla, A., Borghi, N., Bouchet, F.R., Braglia, M., Buchert, T., Buckley-Geer, E., Calabrese, E., Caldwell, R.R., Camarena, D., Capozziello, S., Casertano, S., Chen, G.C.F., Chluba, J., Chen, A., Chen, H.Y., Chudaykin, A., Cicoli, M., Copi, C.J., Courbin, F., Cyr-Racine, F.Y., Czerny, B., Dainotti, M., D’Amico, G., Davis, A.C., de Cruz Pérez, J., de Haro, J., Delabrouille, J., Denton, P.B., Dhawan, S., Dienes, K.R., Di Valentino, E., Du, P., Eckert, D., Escamilla-Rivera, C., Férté, A., Finelli, F., Fosalba, P., Freedman, W.L., Frusciante, N., Gaztanaga, E., Giare, W., Giusarma, E., Gómez-Valent, A., Handley, W., Harrison, I., Hart, L., Hazra, D.K., Heavens, A., Heinesen, A., Hildebrandt, H., Hill, J.C., Hogg, N.B., Holz, D.E., Hooper, D.C., Hosseininejad, N., Huterer, D., Ishak, M., Ivanov, M.M., Jaffe, A.H., Jang, I.S., Jedamzik, K., Jimenez, R., Joseph, M., Joudaki, S., Kamionkowski, M., Karwal, T., Kazantzidis, L., Keeley, R.E., Klasek, M., Komatsu, E., Koopmans, L.V.E., Kumar, S., Lamagna, L., Lazkoz, R., Lee, C.C., Lesgourgues, J., Levi Said, J., Lewis, T.R., L’Huillier, B., Lucca, M., Maartens, R., Macri, L.M., Marfatia, D., Marra, V., Martins, C.J.A.P., Masi, S., Matarrese, S., Mazumdar, A., Melchiorri, A., Mena, O., Mersini-Houghton, L., Mertens, J., Milaković, D., Minami, Y., Miranda, V., Moreno-Pulido, C., Moresco, M., Mota, D.F., Mottola, E., Mozzon, S., Muir, J., Mukherjee, A., Mukherjee, S., Naselsky, P., Nath, P., Nesseris, S., Niedermann, F., Notari, A., Nunes, R.C., Ó Colgáin, E., Owens, K.A., Özülker, E., Pace, F., Paliathanasis, A., Palmese, A., Pan, S., Paolletti, D., Perez Bergliaffa, S.E., Perivolaropoulos, L., Pesce, D.W., Pettorino, V., Philcox, O.H.E., Pogosian, L., Poulin, V., Poulot, G., Raveri, M., Reid, M.J., Renzi, F., Riess, A.G., Sabla, V.I., Salucci, P., Salzano, V., Saridakis, E.N., Sathyaprakash, B.S., Schmalz, M., Schöneberg, N., Scolnic, D., Sen, A.A., Sehgal, N., Shafieloo, A., Sheikh-Jabbari, M.M., Silk, J., Silvestri, A., Skara, F., Sloth, M.S., Soares-Santos, M., Solà Peracaula, J., Songsheng, Y.Y., Soriano, J.F., Staicova, D., Starkman, G.D., Szapudi, I., Teixeira, E.M., Thomas, B., Treu, T., Trott, E., van de Bruck, C., Vazquez, J.A., Verde, L., Visinelli, L., Wang, D., Wang, J.M., Wang, S.J., Watkins, R., Watson, S., Webb, J.K., Weiner, N., Wiltman, A., Witte, S.J., Wojtak, R., Yadav, A.K., Yang, W., Zhao, G.B., Zumalacárregui, M., 2022. Cosmology intertwined: A review of the particle physics, astrophysics, and cosmology associated with the cosmological tensions and anomalies. *Journal of High Energy Astrophysics* 34, 49–211. doi:10.1016/j.jheap.2022.04.002, arXiv:2203.06142.
- Alam, S., Aubert, M., Avila, S., Bolland, C., Bautista, J.E., Bershad, M.A., Bizyaev, D., Blanton, M.R., Bolton, A.S., Bovy, J., Brinkmann, J., Brownstein, J.R., Burtin, E., Chabanier, S., Chapman, M.J., Choi, P.D., Chuang, C.H., Comparat, J., Cousinou, M.C., Cuceu, A., Dawson, K.S., de la Torre, S., de Mattia, A., Agathe, V.d.S., des Bourboux, H.d.M., Escoffier, S., Etourneau, T., Farr, J., Font-Ribera, A., Frinchaboy, P.M., Fromenteau, S., Gil-Marín, H., Le Goff, J.M., Gonzalez-Morales, A.X., Gonzalez-Perez, V., Grabowski, K., Guy, J., Hawken, A.J., Hou, J., Kong, H., Parker, J., Klaene, M., Kneib, J.P., Lin, S., Long, D., Lyke, B.W., de la Macorra, A., Martini, P., Masters, K., Mohammad, F.G., Moon, J., Mueller, E.M., Muñoz-Gutiérrez, A., Myers, A.D., Nadathur, S., Neveux, R., Newman, J.A., Noterdaeme, P., Oravetz, A., Oravetz, D., Palanque-Delabrouille, N., Pan, K., Paviot, R., Percival, W.J., Pérez-Ràfols, I., Petitjean, P., Pieri, M.M., Prakash, A., Rai-choor, A., Ravoux, C., Rezaie, M., Rich, J., Ross, A.J., Rossi, G., Ruggeri, R., Ruhlmann-Kleider, V., Sánchez, A.G., Sánchez, F.J., Sánchez-Gallego, J.R., Sayres, C., Schneider, D.P., Seo, H.J., Shafieloo, A., Slosar, A., Smith, A., Stermer, J., Tamone, A., Tinker, J.L., Tojeiro, R., Vargas-Magaña, M., Variu, A., Wang, Y., Weaver, B.A., Weijmans, A.M., Yèche, C., Zarrouk, P., Zhao, C., Zhao, G.B., Zheng, Z., 2021. Completed SDSS-IV extended Baryon Oscillation Spectroscopic Survey: Cosmological implications from two decades of spectroscopic surveys at the Apache Point Observatory. *prd* 103, 083533. doi:10.1103/PhysRevD.103.083533, arXiv:2007.08991.
- Amendola, L., Kainulainen, K., Marra, V., Quartin, M., 2010. Large-Scale Inhomogeneities May Improve the Cosmic Concordance of Supernovae. *prl* 105, 121302. doi:10.1103/PhysRevLett.105.121302, arXiv:1002.1232.
- Anscombe, F.J., Glynn, W.J., 1983. Distribution of the kurtosis statistic b_2 for normal samples. *Biometrika* 70, 227–234.
- Bargiacchi, G., Dainotti, M.G., Nagataki, S., Capozziello, S., 2023. Gamma-ray bursts, quasars, baryonic acoustic oscillations, and supernovae Ia: new statistical insights and cosmological constraints. *mnras* 521, 3909–3924. doi:10.1093/mnras/stad763, arXiv:2303.07076.
- Brout, D., Scolnic, D., Popovic, B., Riess, A.G., Carr, A., Zuntz, J., Kessler, R., Davis, T.M., Hinton, S., Jones, D., Kenworthy, W.D., Peterson, E.R., Said, K., Taylor, G., Ali, N., Armstrong, P., Charvu, P., Dwomoh, A., Meldorf, C., Palmese, A., Qu, H., Rose, B.M., Sanchez, B., Stubbs, C.W., Vincenzi, M., Wood, C.M., Brown, P.J., Chen, R., Chambers, K., Coulter, D.A., Dai, M., Dimitriadis, G., Filippenko, A.V., Foley, R.J., Jha, S.W., Kelsey, L., Kirshner, R.P., Möller, A., Muir, J., Nadathur, S., Pan, Y.C., Rest, A., Rojas-Bravo, C., Sako, M., Siebert, M.R., Smith, M., Stahl, B.E., Wiseman, P., 2022. The Pantheon+ Analysis: Cosmological Constraints. *apj* 938, 110. doi:10.3847/1538-4357/ac8e04, arXiv:2202.04077.
- Camarena, D., Marra, V., 2020. Local determination of the Hubble constant and the deceleration parameter. *Physical Review Research* 2, 013028. doi:10.1103/PhysRevResearch.2.013028, arXiv:1906.11814.
- Cao, S., Ryan, J., Ratra, B., 2021. Using Pantheon and DES supernova, baryon acoustic oscillation, and Hubble parameter data to constrain the Hubble constant, dark energy dynamics, and spatial curvature. *mnras* 504, 300–310. doi:10.1093/mnras/stab942, arXiv:2101.08817.
- Cardone, V.F., Capozziello, S., Dainotti, M.G., 2009. An updated gamma-ray bursts Hubble diagram. *mnras* 400, 775–790. doi:10.1111/j.1365-2966.2009.15456.x, arXiv:0901.3194.
- Cardone, V.F., Dainotti, M.G., Capozziello, S., Willingale, R., 2010. Constraining cosmological parameters by gamma-ray burst X-ray afterglow light curves. *mnras* 408, 1181–1186. doi:10.1111/j.1365-2966.2010.17197.x, arXiv:1005.0122.
- Carroll, S.M., 2001. The Cosmological Constant. *Living Reviews in Relativity* 4, 1. doi:10.12942/lrr-2001-1, arXiv:astro-ph/0004075.
- Colgáin, E.Ó., Sheikh-Jabbari, M.M., Solomon, R., 2022a. High Redshift Λ CDM Cosmology: To Bin or not to Bin? arXiv e-prints , arXiv:2211.02129arXiv:2211.02129.
- Colgáin, E.Ó., Sheikh-Jabbari, M.M., Solomon, R., Dainotti, M.G., Stojkovic, D., 2022b. Putting Flat Λ CDM In The (Redshift) Bin. arXiv e-prints , arXiv:2206.11447arXiv:2206.11447.
- D’Agostino, R., Pearson, E.S., 1973. Tests for departure from normality. empirical results for the distributions of b_2 and \sqrt{b} . *Biometrika* 60, 613–622.
- D’Agostino, R.B., Belanger, A., Jr., R.B.D., 1990. A suggestion for using powerful and informative tests of normality. *The American Statistician* 44, 316–321. URL: <https://www.tandfonline.com/doi/abs/10.1080/00031305.1990.10475751>, doi:10.1080/00031305.1990.10475751, arXiv:https://www.tandfonline.com/doi/pdf/10.1080/00031305.1990.10475751.
- Dainotti, M.G., Cardone, V.F., Piedipalumbo, E., Capozziello, S., 2013. Slope evolution of GRB correlations and cosmology. *mnras* 436, 82–88. doi:10.1093/mnras/stt1516, arXiv:1308.1918.
- Dainotti, M.G., De Simone, B., Schiavone, T., Montani, G., Rinaldi, E., Lambiase, G., 2021. On the Hubble Constant Tension in the SNe Ia Pantheon Sample. *apj* 912, 150. doi:10.3847/1538-4357/abeb73, arXiv:2103.02117.
- Dainotti, M.G., De Simone, B., Schiavone, T., Montani, G., Rinaldi, E., Lambiase, G., Bogdan, M., Ugale, S., 2022a. On the evolution of the Hubble constant with the SNe Ia Pantheon Sample and Baryon Acoustic Oscillations: a feasibility study for GRB-cosmology in 2030. *Galaxies* 10, 24–66. doi:10.3390/galaxies10010024, arXiv:2201.09848.
- Dainotti, M.G., Lenart, A.L., Chraya, A., Sarracino, G., Nagataki, S., Fraija, N., Capozziello, S., Bogdan, M., 2022b. The Gamma-ray Bursts Fundamental Plane correlation as a cosmological tool. *mnras* doi:10.1093/mnras/stac2752, arXiv:2209.08675.
- Dainotti, M.G., Sarracino, G., Capozziello, S., 2022c. Gamma-ray bursts, supernovae Ia, and baryon acoustic oscillations: A binned cosmological analysis. *pasj* doi:10.1093/pasj/psac057, arXiv:2206.07479.
- Dainotti, M.G., Young, S., Li, L., Levine, D., Kalinowski, K.K., Kann, D.A., Tran, B., Zambrano-Tapia, L., Zambrano-Tapia, A., Cenko, S.B., Fuentes, M., Sánchez-Vázquez, E.G., Oates, S.R., Fraija, N., Becerra, R.L., Watson, A.M., Butler, N.R., González, J.J., Kutryk, A.S., Lee, W.H., Prochaska, J.X., Ramirez-Ruiz, E., Richer, M.G., Zola, S., 2022d. The Optical Two- and

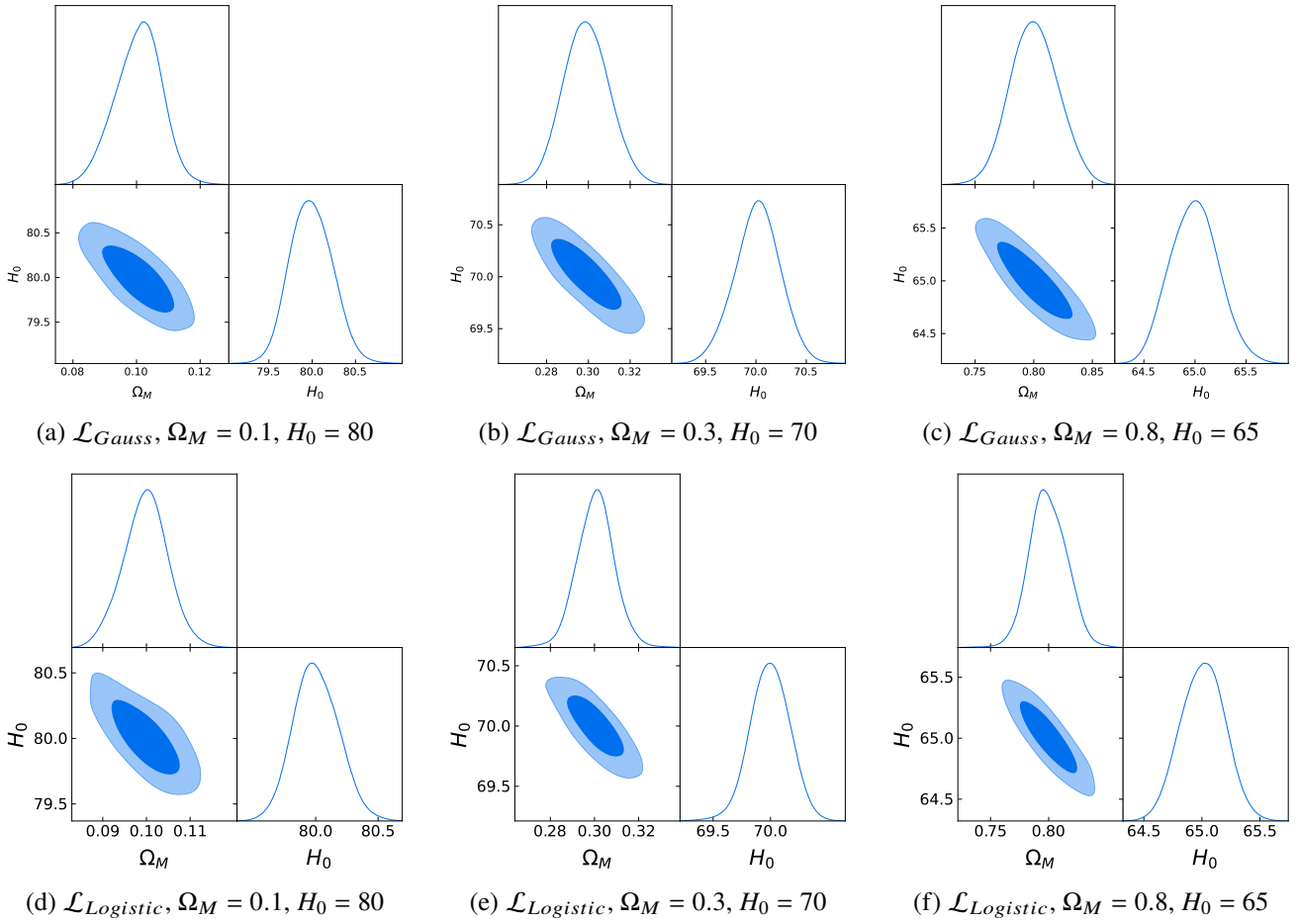


Figure A.4: Fit of the flat Λ CDM model with Ω_M and H_0 free parameters for the mock sample for the Pantheon sample. H_0 is expressed in units of $\text{km s}^{-1} \text{Mpc}^{-1}$.

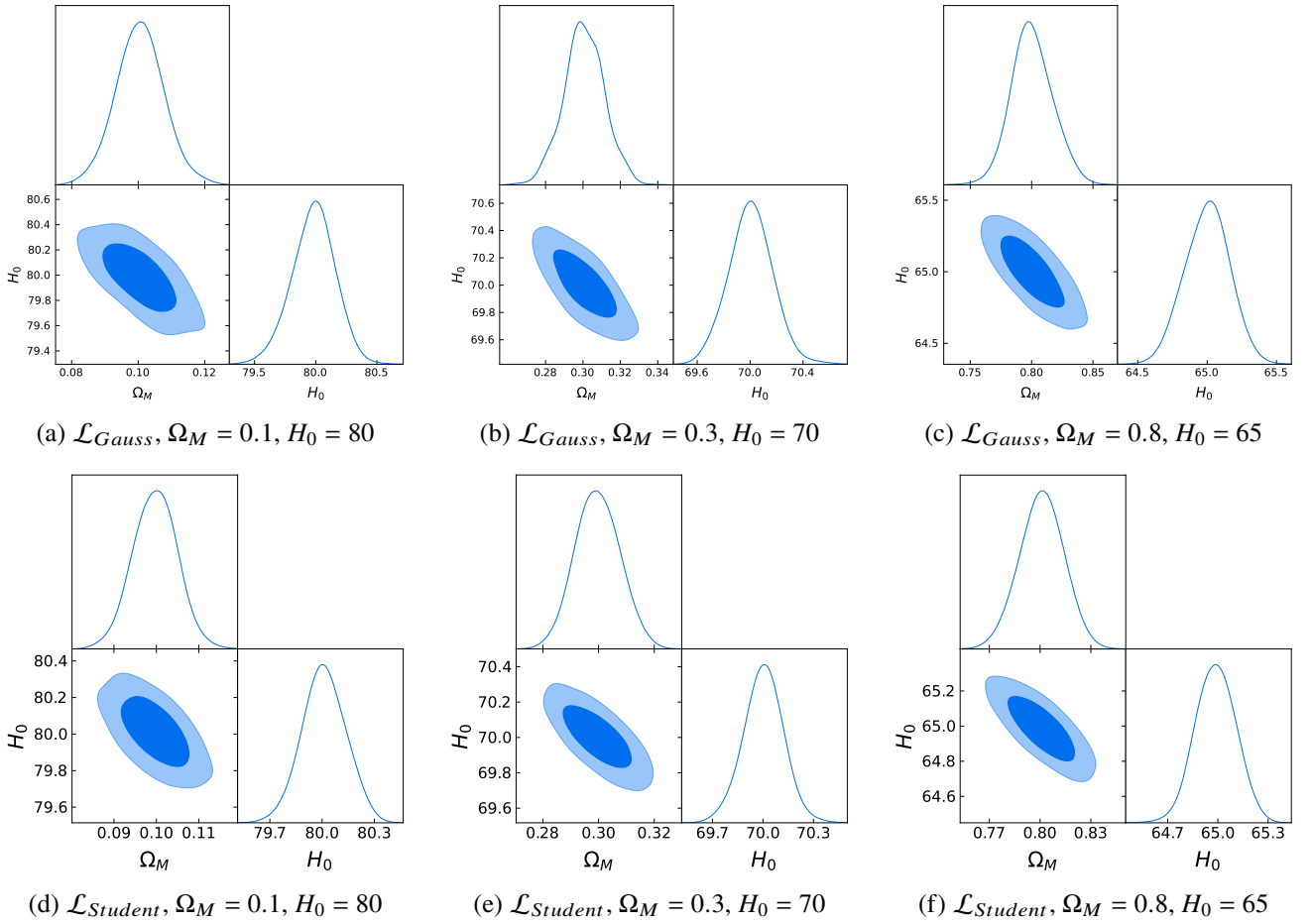


Figure A.5: Fit of the flat Λ CDM model with Ω_M and H_0 free parameters for the mock sample for the Pantheon+ sample. H_0 is expressed in units of $\text{km s}^{-1} \text{Mpc}^{-1}$.

- Three-dimensional Fundamental Plane Correlations for Nearly 180 Gamma-Ray Burst Afterglows with Swift/UVOT, RATIR, and the Subaru Telescope. *apjs* 261, 25. doi:10.3847/1538-4365/ac7c64, arXiv:2203.12908.
- Dempster, A.P., Laird, N.M., Rubin, D.B., 1977. Maximum likelihood from incomplete data via the em algorithm. *Journal of the royal statistical society: series B (methodological)* 39, 1–22.
- Di Valentino, E., Gariazzo, S., Mena, O., Vagnozzi, S., 2020. Soundness of dark energy properties. *jcap* 2020, 045. doi:10.1088/1475-7516/2020/07/045, arXiv:2005.02062.
- Feeney, S.M., Mortlock, D.J., Dalmasso, N., 2018. Clarifying the Hubble constant tension with a Bayesian hierarchical model of the local distance ladder. *mnras* 476, 3861–3882. doi:10.1093/mnras/sty418, arXiv:1707.00007.
- Freedman, W.L., 2021. Measurements of the Hubble Constant: Tensions in Perspective. *apj* 919, 16. doi:10.3847/1538-4357/ac0e95, arXiv:2106.15656.
- Gómez-Valent, A., Amendola, L., 2018. H_0 from cosmic chronometers and Type Ia supernovae, with Gaussian Processes and the novel Weighted Polynomial Regression method. *jcap* 2018, 051. doi:10.1088/1475-7516/2018/04/051, arXiv:1802.01505.
- Hahn, C., Beutler, F., Sinha, M., Berlind, A., Ho, S., Hogg, D.W., 2019. Likelihood non-Gaussianity in large-scale structure analyses. *mnras* 485, 2956–2969. doi:10.1093/mnras/stz558, arXiv:1803.06348.
- Holz, D.E., Linder, E.V., 2005. Safety in Numbers: Gravitational Lensing Degradation of the Luminosity Distance-Redshift Relation. *apj* 631, 678–688. doi:10.1086/432085, arXiv:astro-ph/0412173.
- Jia, X.D., Hu, J.P., Wang, F.Y., 2022. The evidence for a decreasing trend of Hubble constant. arXiv e-prints, arXiv:2212.00238, arXiv:2212.00238.
- Jönsson, J., Sullivan, M., Hook, I., Basa, S., Carlberg, R., Conley, A., Fouchez, D., Howell, D.A., Perrett, K., Pritchet, C., 2010. Constraining dark matter halo properties using lensed Supernova Legacy Survey supernovae. *mnras* 405, 535–544. doi:10.1111/j.1365-2966.2010.16467.x, arXiv:1002.1374.
- Kass, R.E., Raftery, A.E., 1995. Bayes factors. *Journal of the American Statistical Association* 90, 773–795.
- Keeley, R., Shafieloo, A., L’Huillier, B., 2022. An Analysis of Variance of the Pantheon+ Dataset: Systematics in the Covariance Matrix? arXiv e-prints, arXiv:2212.07917, doi:10.48550/arXiv.2212.07917, arXiv:2212.07917.
- Kelly, B.C., 2007. Some Aspects of Measurement Error in Linear Regression of Astronomical Data. *apj* 665, 1489–1506. doi:10.1086/519947, arXiv:0705.2774.
- Kenworthy, W.D., Scolnic, D., Riess, A., 2019. The Local Perspective on the Hubble Tension: Local Structure Does Not Impact Measurement of the Hubble Constant. *apj* 875, 145. doi:10.3847/1538-4357/ab0ebf, arXiv:1901.08681.
- Lenart, A., Bargiacchi, G., Dainotti, M.G., Nagataki, S., Capozziello, S., 2023. A Bias-free Cosmological Analysis with Quasars Alleviating H_0 Tension. *apjs* 264, 46. doi:10.3847/1538-4365/aca404.
- Leslie, J.R., Stephens, M.A., Fotopoulos, S., 1986. Asymptotic distribution of the shapiro-wilk w for testing for normality. *Ann. Statist.* 14, 1497–1506.
- Liao, K., Shafieloo, A., Keeley, R.E., Linder, E.V., 2019. A Model-independent Determination of the Hubble Constant from Lensed Quasars and Supernovae Using Gaussian Process Regression. *apjl* 886, L23. doi:10.3847/2041-8213/ab5308, arXiv:1908.04967.
- Lovick, T., Dhawan, S., Handley, W., 2023. Non-gaussian likelihoods for type Ia supernovae cosmology: Implications for dark energy and h_0 . arXiv:2312.02075.
- Lusso, E., Risaliti, G., Nardini, E., Bargiacchi, G., Benetti, M., Bisogni, S., Capozziello, S., Civano, F., Eggleston, L., Elvis, M., Fabbiano, G., Gilli, R., Marconi, A., Paolillo, M., Piedipalumbo, E., Salvaterra, F., Signorini, M., Vignali, C., 2020. Quasars as standard candles. III. Validation of a new sample for cosmological studies. *aap* 642, A150. doi:10.1051/0004-6361/202038899, arXiv:2008.08586.
- Macaulay, E., Bacon, D., Nichol, R.C., Davis, T.M., Elvin-Poole, J., Brout, D., Carollo, D., Glazebrook, K., Hinton, S.R., Lewis, G.F., Lidman, C., Möller, A., Sako, M., Scolnic, D., Smith, M., Sommer, N.E., Tucker, B.E., Abbott, T.M.C., Aguena, M., Annis, J., Avila, S., Bertin, E., Bhargava, S., Brooks, D., Burke, D.L., Carnero Costa, A., Carrasco Kind, M., Carretero, J., Castander, F.J., Costanzi, M., da Costa, L.N., Desai, S., Diehl, H.T., Doel, P., Flaugher, B., Foley, R.J., García-Bellido, J., Gaztanaga, E., Gerdes, D.W., Gruen, D., Gruendl, R.A., Gschwend, J., Gutierrez, G., Hollowood, D.L., Honscheid, K., Huterer, D., James, D.J., Kuehn, K., Kuropatkin, N., Lahav, O., Lima, M., Maia, M.A.G., Marshall, J.L., Melchior, P., Menanteau, F., Miquel, R., Palmese, A., Plazas, A.A., Romer, A.K., Roodman, A., Sanchez, E., Scarpine, V., Schubnell, M., Serrano, S., Sevilla-Noarbe, I., Soares-Santos, M., Suchyta, E., Swanson, M.E.C., Tarle, G., Varga, T.N., Walker, A.R., Weller, J., DES Collaboration, 2020. Weak lensing of Type Ia Supernovae from the Dark Energy Survey. *mnras* 496, 4051–4059. doi:10.1093/mnras/staa1852, arXiv:2007.07956.
- Peebles, P.J.E., 1984. Tests of cosmological models constrained by inflation. *apj* 284, 439–444. doi:10.1086/162425.
- Perlmutter, S., Aldering, G., Goldhaber, G., Knop, R.A., Nugent, P., Castro, P.G., Deustua, S., Fabbro, S., Goobar, A., Groom, D.E., Hook, I.M., Kim, A.G., Kim, M.Y., Lee, J.C., Nunes, N.J., Pain, R., Pennypacker, C.R., Quimby, R., Lidman, C., Ellis, R.S., Irwin, M., McMahon, R.G., Ruiz-Lapuente, P., Walton, N., Schaefer, B., Boyle, B.J., Filippenko, A.V., Matheson, T., Fruchter, A.S., Panagia, N., Newberg, H.J.M., Couch, W.J., Project, T.S.C., 1999. Measurements of Ω and Λ from 42 High-Redshift Supernovae. *apj* 517, 565–586. doi:10.1086/307221, arXiv:astro-ph/9812133.
- Planck Collaboration, Aghanim, N., Akrami, Y., Ashdown, M., Aumont, J., Baccigalupi, C., Ballardini, M., Banday, A.J., Barreiro, R.B., Bartolo, N., Basak, S., Battye, R., Benabed, K., Bernard, J.P., Bersanelli, M., Bielewicz, P., Bock, J.J., Bond, J.R., Borrill, J., Bouchet, F.R., Boulanger, F., Bucher, M., Burigana, C., Butler, R.C., Calabrese, E., Cardoso, J.F., Carron, J., Challinor, A., Chiang, H.C., Chluba, J., Colombo, L.P.L., Combet, C., Contreras, D., Crill, B.P., Cuttaia, F., de Bernardis, P., de Zotti, G., Delabrouille, J., Delouis, J.M., Di Valentino, E., Diego, J.M., Doré, O., Douspis, M., Ducout, A., Dupac, X., Dusini, S., Efstathiou, G., Elsner, F., Enßlin, T.A., Eriksen, H.K., Fantaye, Y., Farhang, M., Fergusson, J., Fernandez-Cobos, R., Finelli, F., Forastieri, F., Frailis, M., Fraisse, A.A., Franceschi, E., Frolov, A., Galeotta, S., Galli, S., Ganga, K., Génova-Santos, R.T., Gerbino, M., Ghosh, T., González-Nuevo, J., Górski, K.M., Gratton, S., Gruppuso, A., Gudmundsson, J.E., Hamann, J., Handley, W., Hansen, F.K., Herranz, D., Hildebrandt, S.R., Hivon, E., Huang, Z., Jaffe, A.H., Jones, W.C., Karakci, A., Keihänen, E., Keskitalo, R., Kiiveri, K., Kim, J., Kisner, T.S., Knox, L., Krachmalnicoff, N., Kunz, M., Kurki-Suonio, H., Lagache, G., Lamarre, J.M., Lasenby, A., Lattanzi, M., Lawrence, C.R., Le Jeune, M., Lemos, P., Lesgourgues, J., Levrier, F., Lewis, A., Liguori, M., Lilje, P.B., Lilley, M., Lindholm, V., López-Cañiego, M., Lubin, P.M., Ma, Y.Z., Macías-Pérez, J.F., Maggio, G., Maino, D., Mandolesi, N., Mangilli, A., Marcos-Caballero, A., Maris, M., Martin, P.G., Martinelli, M., Martínez-González, E., Matarrese, S., Mauri, N., McEwen, J.D., Meinhold, P.R., Melchiorri, A., Mennella, A., Migliaccio, M., Millea, M., Mitra, S., Miville-Deschênes, M.A., Molinari, D., Montier, L., Morgante, G., Moss, A., Natoli, P., Nørgaard-Nielsen, H.U., Pagano, L., Paoletti, D., Partridge, B., Patanchon, G., Peiris, H.V., Perrotta, F., Pettorino, V., Piacentini, F., Polastri, L., Polenta, G., Puget, J.L., Rachen, J.P., Reinecke, M., Remazeilles, M., Renzi, A., Rocha, G., Rosset, C., Roudier, G., Rubiño-Martín, J.A., Ruiz-Granados, B., Salvati, L., Sandri, M., Savelainen, M., Scott, D., Shellard, E.P.S., Sirignano, C., Sirri, G., Spencer, L.D., Sunyaev, R., Suur-Uski, A.S., Tauber, J.A., Tavagnacco, D., Tenti, M., Toffolatti, L., Tomasi, M., Trombetti, T., Valenziano, L., Valiviita, J., Van Tent, B., Vibert, L., Vielva, P., Villa, F., Vittorio, N., Wandelt, B.D., Wehus, I.K., White, M., White, S.D.M., Zacchei, A., Zonca, A., 2020. Planck 2018 results. VI. Cosmological parameters. *aap* 641, A6. doi:10.1051/0004-6361/201833910, arXiv:1807.06209.
- Postnikov, S., Dainotti, M.G., Hernandez, X., Capozziello, S., 2014. Non-parametric Study of the Evolution of the Cosmological Equation of State with SNeIa, BAO, and High-redshift GRBs. *apj* 783, 126. doi:10.1088/0004-637X/783/2/126, arXiv:1401.2939.
- Razali, N.M., Wah, Y.B., et al., 2011. Power comparisons of shapiro-wilk, kolmogorov-smirnov, lilliefors and anderson-darling tests. *Journal of statistical modeling and analytics* 2, 21–33.
- Riess, A.G., Casertano, S., Yuan, W., Macri, L.M., Scolnic, D., 2019. Large Magellanic Cloud Cepheid Standards Provide a 1% Foundation for the Determination of the Hubble Constant and Stronger Evidence for Physics beyond Λ CDM. *apj* 876, 85. doi:10.3847/1538-4357/ab1422, arXiv:1903.07603.
- Riess, A.G., Filippenko, A.V., Challis, P., Clocchiatti, A., Diercks, A., Garnavich, P.M., Gilliland, R.L., Hogan, C.J., Jha, S., Kirshner, R.P., Leibundgut, B., Phillips, M.M., Reiss, D., Schmidt, B.P., Schommer, R.A., Smith, R.C., Spyromilio, J., Stubbs, C., Suntzeff, N.B., Tonry, J., 1998. Ob-

- servational Evidence from Supernovae for an Accelerating Universe and a Cosmological Constant. *aj* 116, 1009–1038. doi:10.1086/300499, arXiv:astro-ph/9805201.
- Riess, A.G., Macri, L.M., Hoffmann, S.L., Scolnic, D., Casertano, S., Filippenko, A.V., Tucker, B.E., Reid, M.J., Jones, D.O., Silverman, J.M., Chornock, R., Challis, P., Yuan, W., Brown, P.J., Foley, R.J., 2016. A 2.4% Determination of the Local Value of the Hubble Constant. *apj* 826, 56. doi:10.3847/0004-637X/826/1/56, arXiv:1604.01424.
- Riess, A.G., Yuan, W., Macri, L.M., Scolnic, D., Brout, D., Casertano, S., Jones, D.O., Murakami, Y., Anand, G.S., Breuval, L., Brink, T.G., Filippenko, A.V., Hoffmann, S., Jha, S.W., D'arcy Kenworthy, W., Mackenty, J., Stahl, B.E., Zheng, W., 2022. A Comprehensive Measurement of the Local Value of the Hubble Constant with $1 \text{ km s}^{-1} \text{ Mpc}^{-1}$ Uncertainty from the Hubble Space Telescope and the SHOES Team. *apjl* 934, L7. doi:10.3847/2041-8213/ac5c5b, arXiv:2112.04510.
- Risaliti, G., Lusso, E., 2019. Cosmological constraints from the Hubble diagram of quasars at high redshifts. *Nature Astronomy*, 195doi:10.1038/s41550-018-0657-z.
- Sarkar, D., Amblard, A., Holz, D.E., Cooray, A., 2008. Lensing and Supernovae: Quantifying the Bias on the Dark Energy Equation of State. *apj* 678, 1–5. doi:10.1086/586886, arXiv:0710.4143.
- Schiavone, T., Montani, G., Bombacigno, F., 2023. $f(R)$ gravity in the Jordan frame as a paradigm for the Hubble tension. *mnras* 522, L72–L77. doi:10.1093/mnras/1/slad041, arXiv:2211.16737.
- Scolnic, D., Brout, D., Carr, A., Riess, A.G., Davis, T.M., Dwomoh, A., Jones, D.O., Ali, N., Charvu, P., Chen, R., Peterson, E.R., Popovic, B., Rose, B.M., Wood, C.M., Brown, P.J., Chambers, K., Coulter, D.A., Dettman, K.G., Dimitriadis, G., Filippenko, A.V., Foley, R.J., Jha, S.W., Kilpatrick, C.D., Kirshner, R.P., Pan, Y.C., Rest, A., Rojas-Bravo, C., Siebert, M.R., Stahl, B.E., Zheng, W., 2022. The Pantheon+ Analysis: The Full Data Set and Light-curve Release. *apj* 938, 113. doi:10.3847/1538-4357/ac8b7a, arXiv:2112.03863.
- Scolnic, D.M., Jones, D.O., Rest, A., Pan, Y.C., Chornock, R., Foley, R.J., Huber, M.E., Kessler, R., Narayan, G., Riess, A.G., Rodney, S., Berger, E., Brout, D.J., Challis, P.J., Drout, M., Finkbeiner, D., Lunnan, R., Kirshner, R.P., Sanders, N.E., Schlafly, E., Smartt, S., Stubbs, C.W., Tonry, J., Wood-Vasey, W.M., Foley, M., Hand, J., Johnson, E., Burgett, W.S., Chambers, K.C., Draper, P.W., Hodapp, K.W., Kaiser, N., Kudritzki, R.P., Magnier, E.A., Metcalfe, N., Bresolin, F., Gall, E., Kotak, R., McCrum, M., Smith, K.W., 2018. The Complete Light-curve Sample of Spectroscopically Confirmed SNe Ia from Pan-STARRS1 and Cosmological Constraints from the Combined Pantheon Sample. *apj* 859, 101. doi:10.3847/1538-4357/aab9bb, arXiv:1710.00845.
- Shah, P., Lemos, P., Lahav, O., 2023. The impact of weak lensing on Type Ia supernovae luminosity distances. *mnras* 520, L68–L71. doi:10.1093/mnras/1/slad008, arXiv:2210.10688.
- Shapiro, S.S., Wilk, M.B., 1965. An analysis of variance test for normality (complete samples). *Biometrika* 52, 591–611.
- Smith, M., Bacon, D.J., Nichol, R.C., Campbell, H., Clarkson, C., Maartens, R., D'Andrea, C.B., Bassett, B.A., Cinabro, D., Finley, D.A., Frieman, J.A., Galbany, L., Garnavich, P.M., Olmstead, M.D., Schneider, D.P., Shapiro, C., Sollerman, J., 2014. The Effect of Weak Lensing on Distance Estimates from Supernovae. *apj* 780, 24. doi:10.1088/0004-637X/780/1/24, arXiv:1307.2566.
- Stephens, M.A., 1974. Edf statistics for goodness of fit and some comparisons. *Journal of the American statistical Association* 69, 730–737.
- Stephens, M.A., 1976. Asymptotic results for goodness-of-fit statistics with unknown parameters. *The Annals of Statistics* 4, 357–369.
- Stephens, M.A., 1979. Tests of fit for the logistic distribution based on the empirical distribution function. *Biometrika* 66, 591–595.
- Wagenmakers, E.J., 2007. A practical solution to the pervasive problems of p values. *Psychonomic bulletin & review* 14, 779–804.
- Weinberg, S., 1989. The cosmological constant problem. *Reviews of Modern Physics* 61, 1–23. doi:10.1103/RevModPhys.61.1.
- Wong, K.C., Suyu, S.H., Chen, G.C.F., Rusu, C.E., Millon, M., Sluse, D., Bonvin, V., Fassnacht, C.D., Taubenberger, S., Auger, M.W., Birrer, S., Chan, J.H.H., Courbin, F., Hilbert, S., Tihhonova, O., Treu, T., Agnello, A., Ding, X., Jee, I., Komatsu, E., Shajib, A.J., Sonnenfeld, A., Blandford, R.D., Koopmans, L.V.E., Marshall, P.J., Meylan, G., 2020. HOLiCOW - XIII. A 2.4 per cent measurement of H_0 from lensed quasars: 5.3σ tension between early- and late-Universe probes. *mnras* 498, 1420–1439. doi:10.1093/mnras/stz3094, arXiv:1907.04869.
- Yazici, B., Yolacan, S., 2007. A comparison of various tests of normality. *Journal of Statistical Computation and Simulation* 77, 175–183.